# FATIGUE PROPERTIES OF ALLOYS EXHIBITING SPINODAL DECOMPOSITION

# FATIGUE PROPERTIES OF ALLOYS EXHIBITING

### SPINODAL DECOMPOSITION

bу

JOHN TRAVIS PLEWES, B.A.

## A Thesis

Submitted to the Faculty of Graduate Studies
in Partial Fulfilment of the Requirements
for the Degree
Master of Science

McMaster University
May 1966

McMASTER UNIVERSITY Hamilton, Ontario

MASTER OF SCIENCE (Metallurgy)

TITLE: Fatigue Properties of Alloys Exhibiting Spinodal

Decomposition.

AUTHOR: John Travis Plewes, B.A.

SUPERVISORS: Dr. J. S. Kirkaldy, Dr. R. K. Ham

NUMBER OF PAGES: 1x, 60

SCOPE AND CONTENTS:

The mechanical properties of a Cu-2%Co alloy and various CuNiFe alloys have been investigated; in addition, thin film work has been conducted on Superston Bronze and fatigued CuNiFe. The fatigue strengths and ratios of the CuNiFe alloys are comparable to the best of the copper alloys; it was observed that the alloys are considerably better under fatigue conditions for widely varying grain size. The high copper CuNiFe fatigue curves exhibited a pronounced discontinuity, and there appears to be some correlation between abruptness and size of the discontinuity and notch sensitivity. Examination of fatigued CuNiFe indicates that a reversion-reprecipitation-ageing process is occurring, the overall sequence generally being in agreement with the theoretical implications of spinodal decomposition.

# ACKNOWLEDGEMENTS

The author wishes to acknowledge the suggestion and supervision of this problem as well as the invaluable advice provided by Drs. R.K. Ham and J.S. Kirkaldy during this work.

Gratitude is also extended to: Dr. G.P. Contractor of the Dept. Mines and Technical Surveys for providing the use of an extrusion press; Dr. J. McGrath of the Ontario Research Council for supplying 15 pounds of high purity iron; Tono Ojala and Dr. L. Morris of Falconbridge Nickel Mines, Toronto for providing high purity nickel and the use of a vacuum induction furnace and also for performing spectrographic analysis; M. and T. Chemicals Ltd. for providing O.F.H.C. copper; Dr. G.R. Purdy for his assistance with the X.-ray fluorescence unit; and Dr. I. Aitchison for providing the use of his Argon purification train.

The author also wishes to extend his thanks to Drs. Aitchison and Pilliar for their time spent in many hours of valuable discussion.

# TABLE OF CONTENTS

		Subject	Page
Section	1	Introduction	1
	1.1	Fatigue Properties of Al Alloys	1
	1.2	Fatigue Properties of Cu Alloys	3
	1.3	Nucleation/Growth-Spinodal Decomposition	5
	1.4	Review of Previous Work	7
	1.5	Purpose of Investigation	18
Section	2	Experimental	
	2.1	Alloy Preparation	20
	2.2	Heat Treatment	20
	2.3	Tensile and Fatigue Determinations	20
	2.4	Electron Microscopy	21
Section	3	Results and Discussion	
	3.1	Nucleation/Growth vs. Spinodal Decomp.	23
	3.2	Superston Bronze	24
	3.3	Tensile Properties-CuNiFe and CuCo	26
	3.4	Fatigue Properties-CuNiFe and CuCo	29
	3.5	Effect of Grain Size on Fatigue Ratio	30
	3.6	Discontinuity in S.N. Curves	31
	3.7	Fatigued Structure of Annealed CuNiFe	32
	3.8	Fatigued Structure of Swaged CuNiFe	35

		Subject	Page
Section	4	Conclusions	43
Section	5	Suggestions for Future Work	46
Section	6	References	48
Section	7	Appendices	51
	7.1	Alloy Preparation	51
	7.2	Calibration of The Fatigue Machine	54
	7.3	Preparation of Thin Films for E. M.	5 <b>7</b>

•

# LIST OF TABLES

<u>Table</u>	<u>Contents</u>
1	Review of Mechanical Properties of Cu Alloys (1), (60)
2	Heat Treatments and Tensile Properties of
	CuNiFe and CuCo Alloys.
3	Chemical Compositions/Grain Sizes of CuNiFe, CuCo.
4	Fatigue Properties of CuNiFe, CuCo.
5	Review of Mechanical Properties of Superston
	Bronze (1), (57), (58), (59).

# LIST OF ILLUSTRATIONS

Figure	Subject
1.	Effect of grain size on the fatigue strengths for several Copper alloys. (61,62,63)
2.	Apparatus for alloy preparation.
3.	Plot of Dead Weight versus Dynamic Load.
4.	Phase diagram for slow cooled CuNiFe, after Bradley et al (16)
5•	Superston Bronze (typical structure for both heat treatments at low magnifications)
6.	Slow cooled superston bronze; coarsening of random lamellae.
7.	Diffraction pattern of dark phase (foil normal[111]) lamellae traces (Oll).
8.	Diffraction pattern of matrix (foil normal [121]) lamellae traces (010).
9.	Slow cooled Superston bronze, cubic precipitate, cube edges (101) and (101).
10.	Pseudo-binary of $Cu-46\%$ Fe/54%Ni calculated from Bradley et al (16); locus of spinodal calculated as outlined by Cook and Hilliard (51).
11.	Modulation-CuNiFe (heat 7) annealed plus ageing at 640°C/150 minutes. Traces {110}.
12.	Modulation-CuNiFe (heat 7) annealed plus ageing at 640°C/60 minutes. Traces (OII), and (110).
13.	S. N. curve for heat 6, annealed and annealed plus 640°C/90 minutes.
14.	S. N. curve for heat 7, annealed plus 640°C/150 min. (magnification of enclosed pictures x130,000)

# Subject Figure S.N. curve for heat 7, swaged plus 640 C/120 min. 15. (magnification of enclosed pictures, X150,000) 16. S.N. curve for Cu-2%Co (heat 5), annealed plus 640 C/90 min. S.N. curve for heat 8, annealed plus 640 C/3 hours. 17. 18. S.N. curve for heat 9. annealed plus 640 C/3 hours. 19. Microstructure after 167,000 cycles at 39,000 psi (heat 7, annealed plus 640 C/150 minutes) 20. Above specimen, diffraction effect about precipitate. 21. Above specimen, diffraction effect about precipitate. 22. Above specimen, diffraction effect about precipitate. 23. Above specimen, precipitate dislocation interaction. 24. Precipitate after anneal plus 640 C/60 minutes. 25. Microstructure in swaged CuNiFe plus 640 C/2 hours (heat 7) initial modulation present. 26. Above specimen, coarse cell structure. Above specimen, dislocation structure within cell 27. structure. 28. Above specimen, heterogeneous precipitate at grain boundaries. Microstructure in swaged plus 640 C/2 hours after 29. 90,000 cycles at 39,000 psi. Development of cell structure. Above specimen, development of cell structure. 30. 31. Above specimen, coarse cell structure still present. 32. Above specimen, heterogeneous precipitate present at grain boundaries. 33. Above specimen, heterogeneous precipitate present at grain boundaries.

# Figure Subject Twinned area in specimen swaged plus 640°C/2 hours 34. after 90,000 cycles at 39.000 psi. 35. Above specimen, new modulation present. 36. Above specimen, diffraction pattern of modulated area showing typical cellular effect. 37. Above specimen after one month at room temperature, new mode of precipitate present. Microstructure in swaged plus 640°C/2 hours after 38. 370,000 cycles at 39,000 psi, further refinement of cell structure. 39. Above specimen, refinement of cell structure. 40. Above specimen, refinement of cell structure. 41. Above specimen, coarse cell structure still present. 42. Above specimen, new mode of precipitate present. 43. Above specimen, new mode of precipitate present. 44. Above specimen, dislocation pileup at grain boundary.

#### INTRODUCTION

# 1.1 Fatigue Properties of Aluminium Alloys

Because of the importance of the Aluminium alloys in the aircraft industry, their fatigue behavior has received considerable attention and has been comprehensively reviewed by Forrest (1), Templin (2), and Grover (3). Aluminium alloys can be divided into two classes: low and medium strength alloys which depend primarily on alloying elements in solution for their properties, and high strength alloys which are specifically heat treated to develop high strengths by precipitation.

A useful measure of metallurgical and mechanical stability of an alloy under conditions of fatigue is the fatigue ratio, defined as the fatigue strength (at  $10^6$ - $10^8$  cycles) over the ultimate tensile strength. The first group show good fatigue ratios, some showing distinct fatigue limits. Agehardening alloys, on the other hand, continue to slope downwards, even at high numbers of cycles, and exhibit low fatigue ratios. The fatigue ratios for the low strength wrought alloys are comparable with those of the low strength steels, but there is little increase in fatigue strength with increase in tensile strength above about 40,000 psi. The fatigue strengths of the low and medium strength Al alloys can be improved by cold working, however no further benefits are obtained by cold working the age hardening alloys.

At normal temperatures, stable alloys have fatigue ratios of about 0.5. Age hardened Al alloys, however have ratios of approximately 0.3. Orowan (4) suggested that alloys of the latter category (such as Duraluminum) may effectively overage during fatigue. Other workers, Thompson(5), Kennedy (6), Broom et al (7) have considered the fatigue properties of age hardened alloys, and summarize various mechanisms by which effective overageing might occur, and have suggested an alternative softening process; the re-solution of precipitates.

In support of the latter, McEvily et al (8) discovered that a 2024-T4 alloy failed at about  $7 \times 10^6$  cycles at  $2.5 \times 10^4$  psi in rotating bending, but that life was increased to  $18.5 \times 10^6$  cycles for a specimen given an artificial ageing treatment of 16 hours at  $150^\circ$ C after an initial  $0.68 \times 10^6$  cycles. The authors concluded that the softening process occurred in specific slip bands due to re-solution, and that the artificial ageing treatment repairs the damage by reprecipitation of the hardening phase.

For fully age hardened alloys, Hanstock (9) by means of damping measurements on L65 observed no initial hardening but a softening occurring at about 10% of life. Reheating the alloy reduced the damping to its original value as if no cracks were yet present, apparently completely repairing the material. This supports the re-solution theory.

Clark and McEvily (10) investigated Al-4%Cu aged for o"(fully hardened), and found that cyclic strain produced very narrow (1.5 p or less) bands free of precipitate which were full of dislocations. Reageing after fatigue restored the precipitate to its original form. Coffin and Tavernelli (11) found departures from Coffin's law in 2024 alloy and 7075-T6 and attributed this to instability of the precipitates. Abel and Ham (12) investigating Al-4%Cu, did not observe resolution but concluded that failure to do so is explained by the fact that complete resolution is a highly localized process, probably occurring only near the surface at persistent slip bands, and localization of slip is greatly intensified by resolution during fatigue thus causing a low fatigue ratio.

The results for low temperature cycling support this argument. The softening is much more abrupt (since the resolution of precipitate is suppressed due to decreased mobility). Loss of alloy hardening can still occur to some extent by a purely mechanical process (second and third cutting on the same slip plane through a G.P. zone); however the fatigue strength is much increased.

## 1.2 Fatigue Properties of Copper Alloys

The relation between fatigue strength and tensile strength is more variable for copper alloys than for most other metals, as may be seen in table (1). The S. N. curves do not usually show a fatigue limit, and the fatigue strength

appears to be very sensitive to a number of factors; alloy composition, grain size, and the degree of working.

Pure copper has a fatigue strength of only about 6 tons/in<sup>2</sup>. (This is reported both for rotating bending and direct stress (1) at 10<sup>7</sup>-10<sup>8</sup> cycles) This is increased by solid solution hardening as in Cu-Zn and Cu-Sn alloys, but the highest fatigue strengths occur in age hardening alloys such as Cu-2%Be and Superston bronze, although little improvment in fatigue strength is obtained by increasing the tensile strength above about 35 tons/in<sup>2</sup>.

The influence of grain size on the fatigue strengths of copper alloys can be appreciable; refer to figure 1. Comparatively little cold work increases the fatigue strength rapidly, however, further working produces little effect and may even reduce it (13).

Age hardening copper alloys appear to exhibit poor fatigue ratios (0.2-0.4/10<sup>7</sup> cycles) and the general conclusions of resolution in the latter section would appear to also apply (13)

In general then, age hardening Copper and Aluminium alloys produce the highest fatigue strengths but are susceptible to overageing or resolution, and as such exhibit relatively low fatigue ratios.

# 1.3 Nucleation and Growth - Spinodal Decomposition

The classical equilibrium diagram of a binary alloy system shows the boundaries between ranges of homogeneous and heterogeneous equilibrium and their dependence on concentration and temperature. A homogeneous solid solution which on cooling passes such a boundary is assumed to precipitate forming a mixture of two phases with different concentrations. The equilibrium diagram and the equilibrium theory however give no information about the kinetics of the process, or the intermediate states present during precipitation.

As a matter of fact, in the heat treatment of alloys for technical use the objective is very seldom the equilibrium state. Thus, good mechanical properties are connected, for the most part, with some intermediate state, which is thermodynamically unstable, and as such, from a theoretical point of view, the properties should be expected to change with respect to time.

According to generally accepted views, precipitation is ruled by two, more or less independent, phenomena; the formation of nuclei of a new phase, and the growth of these nuclei. There is a tendency for the velocity of growth to increase with increasing temperature due to increased mobility of the atoms. When an alloy is supercooled below the solubility limit into the range of two phase equilibrium, the fluctuations will now and then, at some point give rise

to a state that resembles the equilibrium state and thus will form a stable nucleus that is capable of growing by diffusion processes.

As Gibbs (14) has originally recognized, there are two kinds of infinitesimal changes that may occur in a metastable two component phase. The first is a change that is large in degree, but small in extent; this has givin rise to the well known classical nucleation theory. The second is a change that is infinitesimal in degree but large in extent, as exemplified by a small composition fluctuation spread over a large volume. If a phase is unstable to such a fluctuation, then there is no barrier (other than a diffusional one) to a continuous transformation to a more stable phase.

Solid solutions in which the free energy F varies with composition C such that:

(this is the second case described above) can decompose into a phase mixture with a continuous decrease in free energy. Nucleation is not required, and the precipitation can be homogeneous throughout the whole speciman, ignoring defects, grain boundaries, etc. This type of phase change is known as Spinodal Decomposition.

Within the region of negative to bounded by the

spinodal curve (locus of points plotted on the phase diagram where  $\frac{35}{3c} = 0$ ) the original solid solution is unstable with respect to variations in composition, so that they become accentuated by uphill diffusion.

Unambiguous experimental observations of spinodal decomposition are rare, however an alloy which convincingly exhibits spinodal decomposition is the CuNiFe system.

# 1.4 Review of Previous Work

The CuNiFe system was one of the first ductile magnetic materials to be discovered which had a B.H. product anywhere near that obtained from the brittle AlFeNi alloys. However, the limitations of the system were soon realized, and research was transferred to the AlNiCo alloys.

The CuNiFe system upon slow cooling displayed the interesting phenomenon of X-ray diffraction side bands from which it was postulated that two phenomena were occurring, firstly the formation of a transitional lattice, and secondly the development of a modulated microstructure.

Phase diagrams of the system were first fully investigated by Koster and Dannohl (15) and their results were substantially verified by Bradley, Cox, and Goldschmidt (16). The alloys which developed the highest coercivity lay at room temperature in a two phase region, both phases being F.C.C. with a slightly differing lattice parameter (difference < 1%) while at 950°C, a single F.C.C. phase prevailed.

Interest in the system was stimulated through a discovery by Bradley (16) who noticed that upon slow cooling a sample of  $\text{Cu}_4\text{Ni}_3\text{Fe}$  from its homogenization temperature a transitional precipitate developed prior to the formation of the two equilibrium F.C.C. phases. Analysis of the X-ray powder diffraction photographs showed that certain F.C.C. lines were definitely split, eg. (222) wheras others were not eg. (400), (420). The only possible interpretation was that two finely divided tetragonal lattices were forming, one having an axial ratio just greater, and the other just less than unity. The fact that the (hkO) reflections were sharp and {001} reflections were broadened, suggested that these lattices fitted together as alternating lamellae on the {001} with a common c axis. Further work by Bradley et al (16) indicated that this phenomenon could be detected in alloys covering the complete range of compositions within the two phase range on the equilibrium diagram.

The system was considered by Daniel and Lipson (17) and they assigned the appearance of these sidebands to a regular diffusion of cubic lattices into alternating Cu rich and Cu depleted regions and from comparing two such envisioned periodic variations (one in atomic scattering factor, and the other in lattice parameter by simulating a one dimensional model and calculating the expected diffraction effects) they

were able to postulate that a lattice modulated by sinusoidal lattice parameter changes would account for the observations. The agreement was good for the positions of
the sidebands but less satisfactory when the intensities
were compared.

The measured values of lattice parameters showed differences between the Cu rich and Cu impoverished regions relative to the matrix of -0.7% and +1.7% along the C axis. The wavelength Q of the modulation was found to increase approximately, as given by the equation:

Q = A exp. (function time) + Function (Temp.)
The expression holds only for the intermediate growth stage.
The maximum concentration differences were found to be reached even after the shortest times, this amplitude depending only on the temperature of ageing. Daniel studied in this way uphill diffusion and obtained fair agreement with theoretical results of Becker (18,19).

A rather different interpretation was advanced by Hargreaves (20) using strictly monochromatic radiation to enable very faint diffraction effects to be detected. He amended the sinusoidal modulation model with one composed of a regular arrangement of coherent lamellae of the two metastable tetragonal phases with and without intermediate layers of the parent phase between each pair of lamellae and the waveform was then postulated to be rectangular, that is

Hargreaves thus viewed the decomposition as a precipitate modulating the matrix lattice, the transformation proceeding by a normal nucleation and growth process. Very clear diffraction patterns were obtained and satisfactory agreement between theory and experiment was claimed. However, his experimental work is in some doubt, as results from microscopic examination suffered from the precipitate being too fine to be resolved and results were determined from a general darkening of the etchant to show it up. The asymmetry found in the sidebands was ascribed to the compositions of the alloys investigated as being slightly to one side of the miscibility gap, and this was substantially confirmed both theoretically and experimentally by Balli and Zakharova (21) and by Tiedema, Bouman and Burgers (22).

Geisler (23) investigated some of the well known magnetic materials and included CuNiFe in his study. He examined the structure of the slowly cooled material (which represented a very overaged stage of precipitation) noting a striking Widmanstatten appearance with the plates on {100} habit planes. The effect of cold work was found not only to accelerate the reaction, but also to impart a preferred orientation to the parent grains thus producing an orientation dependance of the precipitation in the direction of rolling. Hibbard (24) found the texture after 95% reduction

by rolling to be (110)[112], (112)[111], (123)[121] but after annealing it became predominately (110)[112] with some (112)[111] present.

Magnetic investigations were carried out by Sucksmith (25) for various times and temperatures and he discovered that the optimum indentation hardness was obtained at a stage when the sidebands were developed and coincided with the maximum B.H. energy product. Similar results were reported by Arndt (26) and Biedermann and Kneller (27). The latter found that the coercive force reached its maximum in a region of rapid increase of the modulation, but before the lamellae were clearly defined. They combined X-ray diffraction with electron microscopy and followed the ageing sequence for a range of alloys, but unfortunately restricted the microscopy to replica techniques which failed to give the necessary resolution for the optimum wavelengths in question.

From the value of the wavelength and details of ternary CuNiFe phase diagrams, they deduced that the shape of the precipitates should be flattened ellipsoids, although Bailey (28) had found in the very high copper alloys evidence for a rod shaped precipitate.

Another extensive investigation was conducted by Pines and Barutkin (29) who used the technique of harmonic analysis on the form of the diffraction lines to determine

the degree of dispersion of the structural constituents and the internal stresses so involved. The microstresses were shown to reach considerable values at the stage when the modulation first became evident, and the peak values of the coercive force coincided with the maximum difference in lattice parameter in accord with the phases still being finely dispersed (the particle size being of the order of 200 A).

The ideas concerning the formation of a modulated lattice have undergone considerable revision in recent years. Geisler (30) dismissed previous theories, and suggested that a copper depleted area would grow and ageing would proceed although he depicted the interzone spacing as remaining constant. Guinier (31) elaborated on this idea. His reasoning was that the periodic lattice previously postulated, should give sharp satellites, whereas the observed satellites had an appreciable width. He thus concluded that the theory of formation of isolated zones (a central lamella of one composition between two lamellae of another composition) was more applicable, and growth could proceed by normal diffusion processes. The diffusion coefficient D is given by the following equation:

D = D, 
$$(C(1-C)/RT)^{2}F/5C^{2}$$

and within the spinodal  $\Im F/\partial C^2$  is negative, and thus D is negative indicating uphill diffusion. This disproves the Guinier model; however it may still apply outside the spinodal although it neither predicts the original widths of the

zones, nor accounts for their initial formation.

The classical concepts of nucleation were first applied to metallic systems by Becker (32) who derived an expression for the interfacial energy between the precipitate and the matrix by considering it as an exchange reaction. Borelius (33) emphasized the importance of gradual changes before attainment of equilibrium and concluded that there should be no barrier to nucleation within the spinodal.

Hillert (34) was able to develop a solid solution model allowing for composition variations in one dimension only (from the zeroth approximation of nearest neighbour interaction) and he used this to calculate the free energy for a series of states in the decomposition of the homogeneous solution. He plotted a free energy surface as a function of wavelength and amplitude and showed that the solution was only unstable to wavelengths greater than a critical wavelength  $\lambda_{\mathbf{c}}$  and that these could increase in amplitude to a metastable state prior to the equilibrium state. The thermodynamic criterion for internal stability yielded a difference equation and one class of solutions was applicable to systems such as CuNiFe. This indicated that a periodic variation of composition modulating the parent lattice was consistent with a reduction of the free energy of the system. The activation energy was shown to

be very low, even well away from the spinodal, so that possibly it was too low to present an effective obstacle to nucleation except for low supersaturations.

The mathematical treatment was later extended to three dimensions by Cahn and Hilliard (35) and their more elaborate equations confirmed the conclusions regarding homogeneous nucleation given by the one dimensional model. They derived an expression for the free energy of a fluid to be:

$$F = \iint \left[ F' + K(\nabla C)^2 \right] dV$$

where v C is the first term of an expansion and is the increase in free energy due to composition gradients, and with this expression, made more rigorous calculations of the critical radii at various supersaturations.

The applicability of this approach to CuNiFe was investigated by Hillert, Cohen, and Averbach (36) by means of X-ray diffraction. They compared the kinetic treatment with the Guinier zone model and from evaluations of the transformation activation energy they showed that both were diffusion controlled inside as well as outside the spinodal, demonstrating that this concept was of no real significance to the nucleation process.

The variation with temperature and composition of the first wavelength to form in the modulated structures was in agreement with the kinetic model and they further proved that a Guinier zone within the spinodal would induce a periodic structure and could thus be a possible mechanism for the initial formation process. They then concluded that the kinetic model was applicable wherever the barrier to nucleation was small and the Guinier model would be restricted to compositions close to the solubility limit.

Cahn (37) developed the theory to take into account the effects of the surface tension and the elastic energy of the precipitate's interface. (as it was well known that these factors would tend to suppress the decomposition) Representing a sinusoidal composition fluctuation with wavelength  $\frac{2\pi}{\beta}$  throughout the homogeneous solid solution of composition  $C_0$  by

$$C = C_0 + A \cos(\beta_1)$$

he calculated the corresponding difference in free energies per unit volume as

$$\frac{\Delta F}{V} = \frac{A^2 \left[ \frac{\lambda^2 F'}{\lambda C^2} + \frac{2\pi^2 E}{(1 - \mu)} + \frac{2k\beta^2}{2} \right]}{2k\beta^2}$$

where  $\eta$  is the linear expansion/unit composition change. Infinite wavelength implies  $\beta = 0$ , so that the condition for instability  $\Delta F = 0$  reduces to

$$\frac{3^2F'}{3C^2} = -2\eta^2E/(1-\mu)$$

which gives the original spinodal condition for  $\eta=0$ . This equation demonstrated that surface tension prevented decomposition of the solid solution on too fine a scale without altering the criterion for stability. Cahn nevertheless

showed that the elastic energy altered the criterion itself by lowering the effective spinodal and necessitated a large degree of supercooling to initiate decomposition. He further deduced that within the unstable area of the phase diagram sufficiently near the limit of metastability the rate of a spinodal mechanism might be too slow to compete with the normal nucleation and growth process.

Cahn (38) also considered the effect of elastic aeolotropy in the early stages of decomposition in a crystal of cubic symmetry. He concluded that provided

(a condition holding for most common metallic systems), where the Young's Modulus is a minimum along the <100>, the solution would first become unstable to fluctuations of composition along these directions and the kinetics would control the growth such that one specific wavelength would predominate giving rise to almost pure sinusoidal modulations of  $\lambda = \mathcal{C} \lambda_c$ . The microstructure would then develop from a simple cubic array of roughly spherical nuclei to two interlocking continuous networks of <100> orientated rods, one enriched and the other impoverished in one of the components. He pointed out that during the initial stages, the amplitude of the individual waves was only one third that of maximum C and that while coherency was maintained

this fraction remained less than 7/8 to that the sidebands could only represent a part of this actual difference.

Further work by Cahn (39) dealt with the hardening expected from such a mode of precipitation. He calculated the force experienced by a dislocation from both the internal stresses and the composition gradients, and concluded that the contribution of the latter was insignificant except where the symmetry reduced the component produced by internal stresses to zero. The dislocations would be expected to wrap themselves around the composition fluctuations as the force amplitude increased and thus would be difficult to detect by direct observation.

Tufton (40) appears to be the only researcher who has incorporated transmission electron microscopy to comprehensively study the early stages of spinodal decomposition. He encountered great difficulty in the preparation and subsequent thinning of the thin foils but was able to gather enough information to describe the ageing sequence. At short times at temperature, a nearly spherical array of particles was present; there did not appear to be any preferred orientation to the particles. Further ageing caused the particles to link together to form rods which coarsened at the expense of their number and shape anisotropy. The sets of adjacent rods then spread laterally to form lamellae

(this corresponding presumably to a slightly tetragonal structure).

This is in opposition to X-ray diffraction results previously reviewed, which suggest that the development of platelets occurred from the very beginning. In Tufton's work, the rods usually showed traces accurately along <110> directions which also is in opposition to theory. (Tufton concluded that the strains were high enough in the foil to cause rumpling to occur, and this was the reason why stereograms did not evince the expected <100>)

# 1.5 Purpose of Investigation

The ultimate aim of the program is to demonstrate fundamental principles which may be applied to the design of a real material and to condition of service.

In this case, the particular aspect of the general problem to be considered is the stability of spinodal decomposition products under conditions of mechanical fatigue. Since spinodal decomposition occurs with a continuous reduction in free energy, it should, in theory be superior to nucleation and growth type decomposition. The argument is as follows.

The very fine scale of spinodal decomposition, the considerable free energy changes involved, and the lattice strains developed all suggest that the process may lead to a very useful strengthening effect in a suitable alloy.

No systematic experimental investigation of this hardening appears to have been published, although several important age hardening alloys may, in fact, develop their strength in this way. The great point of interest is the stability of the decomposition products. As has been previously discussed, in many age hardening nucleation and growth type alloys, the precipitates are thermodynamically unstable. The precipitate structure changes and the alloy is weakened. Fatigue work indicates that precipitates may redissolve during cycling and this would appear to account for the disappointing fatigue properties of alloys of this type. Alloys hardened by spinodal decomposition should be more resistant to such a process since, in theory, the precipitates cannot redissolve. Only the wavelength and amplitude of the composition variations can change. As a result, the strength of such alloys is likely to be relatively stable under fatigue conditions even at elevated temperatures.

It is the specific purpose of this program to test this idea, and to determine the extent of the stability of this form of alloy strengthening under fatigue conditions.

#### EXPERIMENTAL

# 2.1 Alloy Preparation

Four pound heats of CuNiFe, two pound heats of CuCo and a 100 gram heat of Superston bronze were prepared incorporating a 30 KW induction unit and a specially designed apparatus to ensure high purity. Heats were deoxidized with Carbon and/or Aluminium. (Alloy preparation is discussed more fully in Appendix A).

The heats were cast in the form of rods, 0.1"-0.6" in diameter by roughly 12" in length. These were in turn swaged approximately 50% and then solution treated at 975°C for 2 hours (under Argon). This ensured complete homogenization and small grain size. (Refer to table 3 for chemical compositions and grain size). The material was then swaged to a final diameter of 0.25".

# 2.2 Heat Treatment

The 0.25" diameter rod was sectioned into 2.5" length pieces. A proportion of this was further swaged to 0.1" diam. and this was sectioned to 2" pieces. (for tensile determinations). All material was annealed and precipitation treated under Argon at various temperatures and times (Table 2).

## 2.3 Tensile and Fatigue Determinations

All tensile tests were performed on the Instron incorporating modified grips to ensure no slippage. The fatigue properties were determined by incorporating a Baldwin fatigue machine of the axial load or direct stress type. The dynamic force is obtained with an eccentric driven at 2000 rpm operating through a spring in series with the specimen. After calibration (Appendix B)  $\pm 1\%$  applied load was ensured. It was also possible to readjust under dynamic load to ensure equal tensile and compressive load cycles to  $\pm 1\%$ .

Fatigue specimens were of the constant radius type 2.5" in length with 3/4" grips at each end. Minimum diameter was 0.125". Before fatiguing, the specimens were electropolished (Appendix C). It was necessary to grind the surface after heat treatment with 600 grit paper before polishing, to ensure good results.

# 2.4 Electron Microscopy

Considerable difficulty has been encountered previously in the preparation of suitable thin foils of CuNiFe. All electropolishing techniques involved the formation of a film by some corrosive chemical agent and the removal of it by an electrochemical action, and unfortunately, CuNiFe gives an exceedingly tenacious film. Tufton (40) had partial success, but films produced were thin enough for transmission only at the extreme edge of the foils.

A polishing solution has been found which gives very good foils uniformly thin over large areas. (Appendix C)

The same solution, with slight modifications could be used for all compositions of CuNiFe investigated, Cu-2%Co alloys,

and superston bronze.

Fatigued structures were also investigated by cutting the fatigued specimens (with a modified continuous spark cutting arrangement) into discs 0.125" in diameter by 5-15 mils thick.

#### RESULTS AND DISCUSSION

# 3.1 Nucleation and Growth - Spinodal Decomposition

The ultimate aim of this investigation is to determine fundamental principles which may be applied to the design of a real material and its conditions of service. In this case, the particular aspect of the problem to be considered is the stability of spinodal decomposition products under conditions of mechanical fatigue. Since spinodal decomposition occurs with a continuous reduction of free energy, the fatigue properties of alloys exhibiting such precipitation appear, in principle, likely to be superior to those of alloys containing precipitation of the nucleation and growth type.

Unambiguous experimental observations of spinodal decomposition are rare. An alloy which convincingly exhibits this mode of decomposition is the CuNiFe series, which as a result, was chosen for this study. The phase diagram of this system has been described by Bradley, Cox and Goldschmidt (16) and has been reproduced in figure (4). Alloys falling within the two phase region exhibit spinodal decomposition. (16).

An alloy exhibiting precipitation of the nucleation and growth type was also investigated. Many systems of this type were considered (Al-4%Cu, Cu-2%Be etc) but these are usually heat treated at relatively low temperatures (100-300C) indicating that high mobilities are involved. The CuCo system

on the other hand is precipitation treated within the range  $600^{\circ}\text{C-}750^{\circ}\text{C}$  indicating somewhat similar diffusion rates as the CuNiFe system, and was thus chosen as a standard for comparison for fatigue ratios.

## 3.2 Superston Bronze

On reviewing the literature, the highest fatigue ratios of the class two type have been reported for Superston bronze. (table 5) Since this alloy is a CuNiFeAl alloy, it was postulated that this may be an example of spinodal decomposition.

The Aluminium-Bronzes are high copper alloys containing 4-10% Al; additions of Fe, Ni, Si and Mn are frequently made to increase the strength and hardness. The industrial use of Al bronzes is largely restricted to castings of corrosion resistant components and can be divided metallurgically into two types; the alpha or single phase alloys of lower Al content, and alpha-bets or duplex alloys (77%). Under equilibrium conditions, 9.8% Al is soluble in Copper, but this is never obtained in practice; alloys containing greater than 7.5% Al usually exhibiting a duplex structure.

Duplex alloys possess very high tensile properties, but are lacking in ductility. Standard heat treatments involve quenching in water from 1500-1700°F and re-annealing at temperatures between 700-1100°F for 1-2 hours. There is considerable disagreement in the literature with respect to

the mechanical properties of the duplex alloys. There is some evidence that ultimate tensile strengths are little affected by heat treatment; however fatigue properties do show some improvement. The most reliable values of the mechanical properties for the high Al duplex alloys are reproduced in table (5).

A 100 gram heat of Cu-10%Al,5%Fe,5%Ni was prepared and examined by electron microscopy. The material was very brittle and it was necessary to prepare the foils by rolling at bright red heat. Two heat treatments were investigated; as quenched from 850°C in brine, and furnace cooled at aproximately (15°C/min.). The typical structure observed at low magnifications for both heat treatments is shown in figure (5).

At these magnifications, the only difference observed between the two heat treatments is a coarsening of random lamellae in the furnace cooled specimen (figure 6). The structure is typical of a discontinuous eutectoid type of decomposition. A typical diffraction pattern of the dark phase is shown in figure (7); foil normal is [121]. The phase is B.C.C. with a lattice parameter of 2.86 A; lamellae traces are consistent with those of (Oll) planes. The matrix (diffraction pattern, figure 8) shows a foil normal of [121] and is F.C.C. with a lattice parameter of 3.52 A. Lamellae traces are consistent with those of (Olo)

planes. The matrix/lamellae interface thus had (010)//(011).

Barrett (41) reports that Cu-10%Al shows (100)//(110).

The slow cooled matrix also exhibited at high magnifications a cubic semi-coherent precipitate. Fig. (9) shows dislocation interaction with these precipitates; the cube edge traces are consistent with those of (101) and (101) planes.

It is concluded that superston bronze does not exhibit spinodal decomposition but realizes its superior fatigue properties in some undetermined manner, possibly through stability of the cubic precipitate.

# 3.3 Tensile Properties of CuNiFe

A review of the literature reveals very little information regarding the mechanical properties of the CuNiFe alloys. The bulk of the information published (42),(43) pertain to the iron rich end of the phase diagram, falling outside the spinodal region. It is reported by these authors that up to 0.2% carbon can be incorporated without affecting the ductility of the material. This would then indicate that oxygen impurities caused the observed intergranular fractures.

Heat one was found to fail intergranularly after all precipitation treatments. Heat two could be precipitation treated at 810°C for short periods of time, failing transgranularly in tension. However this temperature corresponds to a relatively small concentration amplitude (figure 10)

resulting in a small degree of hardening.

As the purity of the melts increases (heats 6,7,8,9) the tensile properties decrease with a corresponding great increase in ductility. All fractures were transgranular. It was now possible to realize the full hardening potential by precipitation heat treatments at low temperatures producing high concentration amplitudes. However the increase in tensile properties realized from the optimum heat treatments (640°C/1-3hrs) was much smaller than one would expect. Comparing the maximum tensile properties of heat 6 at 640°C to Hillert et al (36) it may be concluded that optimum properties correspond to a modulation wavelength of approximately 100 atomic planes (360 A). However, subsequent electron microscopy performed by the author on this material showed a modulation wavelength of roughly 220 A. The typical structure present is shown in figure (II).

It was observed that optimum tensile properties could be obtained by heat treatments at 640°C for 1-3 hours. Corresponding electron microscopy however shows radically different structures that were observed after one hour (figure 12) and two and one half hours (figure 11).

The ageing sequence thus appears to be as follows: roughly spherical particles grouped rather haphazardly which link up to form rods which in turn coarsen. We are thus in

agreement with the general ageing sequence outlined by Tufton; however it took much longer to develop the same structure in this investigation. (Tufton reports the linkage occurring after 45 minutes at 600°C; we find that 90 minutes at 640°C is required). Tufton reports that he could find no particular preferential grouping for the particles; however if very thin areas of the films are examined, (figure 12) one can distinguish a tendency towards preferential alignment. This picture shows (011) and (110) traces.

Usually, the rods were always perpendicular, irrespective of foil orientation and did not lie in the expected {001}. In this investigation, stereograms always
showed precipitation accurately along {110}. This is in agreement with Tufton, but at odds with theories previously
outlined.

Heats 8 and 9 showed slightly improved U.T.S. values but also did not evince the expected increase in hardening from the ageing treatments. It would appear that the greatest effect of heat treatment was an improvement in the elastic limit.

The Cu-4%Co alloys (heat 4) showed very good benefits from the ageing treatments but were very susceptible to overageing. It was found that it was necessary to solution treat the material approximately 50°C below the liquidus temperature and as a result severe porosity developed in the fatigue specimens. A heat of lower cobalt content was made such that a

a lower annealing temperature could be employed thus restricting any porosity development. The U.T.S. values obtained for the lower cobalt contents in heat 5 were significantly lower than those of heat 4.

It is concluded that spinodal decomposition is not a good hardening mechanism, but that there is some indication that oxygen free carbon bearing CuNiFe may realize significantly greater tensile values.

# 3.4 Fatigue Curves of Cu-2%Co and CuNiFe

The fatigue data for Cu-2%Co (heat 5) and CuNiFe (heats 6,7,8,9) are presented in table (4) and figures (13,14,15,16,17,18) in the form of Stress/ln. No. Cycles.

A review of the literature did not show any fatigue data for the copper cobalt alloys. The material exhibits the typically poor S.N. curves consistent with the class two type of non-ferrous alloy, in which overageing or resolution occurs. The curve shows a fatigue ratio of 0.36 at  $10^6$  cycles and suggests a fatigue "limit" at approximately ten thousand psi. (figure 16)

Heat 6 was lightly swaged and annealed to produce a large grain size (1.5 mm). Two heat treatments were investigated; as annealed, and annealed plus 640°C/90 minutes. The S.N. curves are presented in figure (13) and indicate fatigue ratios of 0.41 and 0.48 respectively at 10<sup>6</sup> cycles.

Heat 7 was heavily swaged and annealed at 1800°F for two hours; half of the heat was then aged at 640°C for two and one-half hours, the remaining half was further swaged and then aged at 640°C for two hours. Grain size for both was approximately 0.04 mm and the S.N. curves are presented in figures (14) and (15) respectively. These treatments were investigated more thoroughly than the others and it was discovered that a discontinuity existed in the fatigue curves at approximately 10<sup>5</sup> cycles. Fatigue ratios at 10<sup>6</sup> cycles were 0.43 for the swaged material and 0.50 for the annealed material.

Heats 8 and 9 were heavily swaged and then annealed at 1850°F for two hours; the material was then aged at 640°C for three hours. This produced an average grain size of 0.06 mm for both heats. The S.N. curves are reproduced in figures (17) and (18) for heats 8 and 9 respectively. Both curves show indications of a definate fatigue limit at 10<sup>6</sup> cycles. The high Fe heat showed the best fatigue ratio of 0.53; the high Ni heat showed a fatigue ratio of 0.50. It should be noted however, that fewer fatigue runs were conducted for these heats and the curves presented are thus only general outlines.

## 3.5 Effect of Grain Size

Copper alloys are notably susceptible to grain size effects under fatigue. Typical effects for some copper alloys

for varying grain size are shown in figure (1). Comparing the fatigue ratios of the CuNiFe, figures (13) and (14), one may conclude that this alloy is considerably better under conditions of fatigue for widely varying grain size.

## 3.6 Discontinuity in S.N. Curves

A search of the literature indicates that this phenomenon has been observed in various non-ferrous alloys between  $10^4$ - $10^6$  cycles. (44,45,46,47,48)

The general consensus falls into two schools of thought. The first is that the S.N. curves are, in reality, a composite of two separate curves with a different fatigue fracture criterion for each. Evidence of the existance of two fracture mechanisms dependent on stress level has been reported in copper and duraluminium, (46). The second school Mori (44) Panseri et al (45) have reported similarly shaped curves and explain the hump by saying that over a certain stress range, local structural modifications are produced by fatigue stressing and these lead to reprecipitation and strengthening of the material in turn resulting in a decreased crack propagation rate. A modification of this theory has been presented by Oding (47) who postulates that the nucleus of a fatigue crack could be formed either by coagulation of vacancies or by their precipitation at favourably situated micropores. Present results indicate humps in

figures (13,14,15). It can be seen however, that the larger grain size fatigue curve is accompanied by a much smaller hump. It has been reported that notch sensitivity increases with decreasing grain size: cold working also increases notch sensitivity (49,50). The greatest and most abrupt hump occurs in small grained swaged CuNiFe which would also have the highest notch sensitivity of the three. Conversely, the smallest hump occurs in the annealed large grained CuNiFe. It would then appear, that there is some correlation between notch sensitivity and the magnitude of the discontinuity as exemplified by the present results for CuNiFe.

There is evidence (section 3.8) that reprecipitation is occurring during fatigue in CuNiFe. Thus it would appear that the reprecipitation hypothesis previously mentioned would account for the observed discontinuity by strengthening the matrix (and thus decreasing the crack propagation rate).

# 3.7 Fatigue Structure of Annealed CuNiFe (heat 7)

A fatigue specimen was prepared, annealed and aged (figure 14). The specimen surface was electropolished, and the sample was then fatigued at  $\pm 39,500$  psi for 167,000 cycles.

The initial modulated structure is shown in fig. (11). It should be noted that this alloy is asymmetrical on the pseudo-binary diagram, figure (10), (locus of spinodal cal-

culated as outlined in (51) ) and thus it is important that measurements of modulation should include both the Cu rich and Cu impoverished segments. (In figure 11, wavelength is measured to be 235 A; Cu rich 185 A. Cu poor 50 A.)

Discs approximately 5 mil thick were sectioned from the fatigued zone incorporating a modified continuous spark cutting arrangement (52). The typical structure observed is shown in figures (19), (20), (21), (22). Zones are approximately 170-190 A. It was observed that the different diffraction effects shown were dependent on the foil orientation. In addition, different areas showed different numbers of precipitates/unit area (figure 19 shows a much higher no. relative to figure 22). It was also observed that a great variation of ultimate contrast, independent of foil orientation was obtained in different areas. This would indicate a variation of ultimate contrast-(concentration amplitude) was present throughout the specimen. In general, it was not possible to orientate the foil such that both dislocations and precipitates could be simultaneously observed. Figure 23 shows a typical dislocation network. Faint images of the precipitate can be resolved in some areas of the picture.

It is concluded that the initial modulation present before fatigue has been partially destroyed resulting in the semi-spherical zones observed. In annealed material subjected

to fatigue, slip becomes localized, and the thin films observed were not from regions of intensified slip. Initially, however slip is uniform and the modulation has been partially destroyed. It is interesting to compare this fatigued structure to the ageing sequence previously outlined. Cunife aged for 1 hour at 640°C displays the structure shown in figures (12), (24). However there is a growth tendency in {110} planes, and the number of precipitates/unit area is much higher than in the fatigued structure. The rods initially present are reverting back to semi-spherical zones.

Calculations presented in section 3.8 show that the minimum wavelength thermodynamically stable at room temperature is of the order of 25-30 A. As dislocations pass through the precipitate during fatigue, relative displacement of any particular rod will continue to occur. With enough displacement, this "bridge" will eventually become less than 30 A and will thus dissolve resulting in the isolated "islands" of precipitate observed. This would also explain the relatively fewer numbers of precipitates, (a proportion of the original modulation completely redissolving) and the variability in ultimate contrast obtained. (a displacement in modulation parallel to the foil surface and perpendicular to the precipitate direction)

# 3.8 Fatigue Structure of Swaged CuNiFe (heat 7)

A portion of heat 7 was heavily swaged, annealed at  $1800^{\circ}F/2$  hours to produce a fine grained structure, and further swaged (90% reduction). The material was then aged at  $640^{\circ}C/2$  hours to produce the optimum modulated structure. Two specimens were electropolished and fatigued at  $\frac{1}{2}$ 39,000 psi for 90,000 and 370,000 cycles respectively. Thin films were sectioned (as previously outlined) from the end and the fatigued area of the specimens.

Typical modulated structures initially present is shown in figure (25). The matrix shows a coarse dislocation cell structure, figure (26) and, at higher magnifications, a dislocation substructure, figure (27). In addition, heterogeneous precipitation is observed at random grain boundaries, as shown in figure (28).

The specimen fatigued for 90,000 cycles shows some development of the cell structure, figures (29),(30). However, some areas still show the original woolly structure still present, figure (31). The heterogeneous precipitate has not changed, figures (32),(33) indicating that the fatiguing has not influenced this effect. Twins were not observed to any great extent, however occasionally small areas did exhibit heavy twinning, figure (34).

It was considered surprising that no remnants of the original modulation were observed; with improved foil preparation techniques it was possible to resolve a new modulation on a much finer scale, in a few isolated areas figure (35). Foil tilting was critical in order to resolve this phase, the modulation usually being observed only in small regions of the overall area. The diffraction pattern of this area, figure (36) shows the typical cellular pattern observed throughout the specimen.

A thin film of this material was prepared and examined after approximately one month at room temperature and a new mode of precipitate was observed, figure (37).

The specimen fatigued for 370,000 cycles shows further refinement of the cellular structure, figures (38),(39),(40). In a few small areas, the original woolly structure was still observed, figure (41). A new precipitate was observed throughout the specimen, figures (42), (43) which is very similar to the one month ageing precipitate, figure (37). A typical dislocation grain boundary effect is shown in figure (44).

Cold worked material softens when subjected to fatigue conditions: slip does not become nearly so localized as in annealed material, and a prominent cell structure develops everywhere. As a result, the modulation

is subjected to more intense slip throughout the fatigued zone, and the modulation completely re-dissolves as
previously discussed. However, due to the great vacancy
production during fatigue, and the thermodynamic implications of spinodal decomposition, reprecipitation occurs
during the fatiguing of the specimen.

The minimum wavelength thermodynamically stable at room temperature can be calculated by combining Cahn's three dimensional dynamic theory with the classical zeroth approximation model. (Cahn's kinetic model can not be incorporated as it applies only to small amplitudes, ie  $\Delta C \ll C$ )

Cahn derived his instability equation (which considers both strain energy and incipient surface energy terms) to be the following:

$$\frac{\Delta F}{V} = \frac{A^2}{4} \left[ \frac{3^2 F}{3 C^2} + \frac{2 \pi^2 E}{1 - \mu} + 2 k \beta^2 \right]$$

Now, for conditions of instability, the bracketed term is just negative, ie:

$$\frac{\delta^2 F}{\delta C^2} \leq -\left[\frac{2\pi^2 E}{1-\mu} + 2k\beta^2\right]$$

From the zeroth approximation model,

$$\frac{\partial^2 F}{\partial C^2} = N_V \left[ \frac{K T}{C(1-C)} - 2 Z J \right]$$

The zeroth approximation model assumes that the interaction energies of components A and B are equal. In the case of CuNiFe, the alloy can be considered as a pseudo-binary of

Cu and NiFe (refer to figure 10). However this phase diagram is calculated to be slightly asymmetric, indicating slightly differing interaction energies. For the following calculation however, they shall be considered equal.

Now, for 
$$T_e$$
,  $\frac{3^2 F_h}{3 e^2} = 0$ 

$$\frac{13^2 F}{N3 C^2} = 0 = \frac{-zZJ + KT}{c(1-C)}c$$
and thus:  $T_e = CzZJ (1-C)/K$ 

$$\frac{3^2 S}{3 c^2} = N_V \left[\frac{KT}{C(1-C)} - zZJ\right]$$

$$= N_V \left[\frac{KT}{C(1-C)} - zZJ\right]$$

$$= N_V \left[\frac{KT}{C(1-C)} - zZJ\right]$$

$$= \frac{N_V K T}{C(1-C)}$$

Equating the second derivatives of the free energy terms:

$$\frac{N_{v}K\Delta T}{C(1-C)} = \frac{2\pi E}{1-\mu} + \frac{2 k \beta^{2}}{1-\mu}$$
or, 
$$\beta = \left[\frac{\pi}{\lambda}\right] = \frac{N_{v}K\Delta T}{2kC(1-C)} - \frac{\pi E}{k(1-\mu)}$$

$$N_{v} = \text{number of atoms/unit volume} \approx 1/a^{2}$$

$$k = 2k T_{c} 3/2 \text{ and for f.c.c.} 2/3 = 3$$
Thus, 
$$\left[\frac{\pi}{\lambda}\right]^{2} = \frac{1}{T_{c}} \left[\frac{2\Delta T}{a^{3}C(1-C)} - \frac{3\pi E}{2K(1-\mu)}\right]$$

From the literature, (16),(35) and from present results, these values can be estimated:

 $T_c = 1233$ °K, T = 298°K, C = 0.4 moles,  $E = 1.7 \times 10^7$  $\eta = 0.04$  A/0.7 moles, h = 1/3,  $k = 1.38 \times 10^{-16}$  erg/deg. Substituting these in the derived equation,

$$\lambda_c = 25-30 \text{ A}$$

Calculations made from figure (35) indicate a wavelength of roughly 65 A. This would indicate that the observed modulation is thermodynamically possible from the classical standpoint. The kinetic aspects of the problem during fatigue can now be considered by employing the relationship of Seitz (53) and Mott (54):

$$D = A la^2 \delta ZC_v exp (-Q_m /kT)$$

where A is an entropy factor = 3, a is the nearest neighbour distance,  $\delta$  is the frequency of lattice vibration, Z is the coordination number = 12,  $C_v$  is the mean concentration of vacancies during fatigue,  $Q_m$  is the activation energy to move a vacancy in the alloy, and kT = 1/40 electron volt. Seitz (53) concluded that the concentration of vacancies is given approximately by:

where E is the total integrated plastic strain. This can be estimated in the following way: (or more precisely as by Coffin (55))

The plastic portion is then estimated to be roughly 1% of this. Thus the plastic strain amplitude per cycle is of the order of 2.35X10<sup>-5</sup>. Total plastic strain after 90,000 cycles is then:

$$= 2NE_{p}/cyclx$$

$$= 2X90,000X(2.35X10^{-5})$$

$$= 4.2 = Ex$$

However, the slip is concentrated only in active persistent slip bands 75% of the volume. Thus in a persistent slip band,  $\epsilon_x = 4.2/0.75 = 5.6$ , and substituting back into our original equation (and assuming that the vacancy production per unit strain is of the same order of magnitude in fatigue)

$$c_v = 5.6 \times 10^{-4}$$

Now the bracketed term in the diffusion equation is simply  $D_{\bullet}$ , and by considering values of  $D_{\bullet}$  for Cu in Ni, (56) one can then calculate  $\delta$ , which is approximately equal to  $1.5 \times 10^{14}$ . D is then calculated to be:

$$D = 3 (2.55 \times 10^{-8}) \times 1.5 \times 10^{14} \times 12 \times 5.6 \times 10^{-4} \exp(-\frac{\pi}{k}T)$$
$$= 3.28 \times 10^{-4} \exp(-\frac{\pi}{k}T)$$

 $Q_{\rm m}$  is the activation energy to move a vacancy in electron volts. Taking  $Q_{\rm m}$  to be roughly 1/3 Q, where Q is the mean activation energy for diffusion in CuNiFe (35), we obtain  $Q_{\rm m}$  to be 55,000/3 = 18,300 calories/gram mole, which is 0.8 electron volts. Thus;

$$D = 3.28 \times 10^{-4} \exp (-0.8/1/40)$$
$$= 3.28 \times 10^{-18} \text{ cm}^2/\text{second}$$

The mean distance for diffusion is given approximately by the relationship:

$$X = \sqrt{2DT}$$

where T is the total time elapsed during fatigue which is roughly 60 minutes, thus:

$$x = \sqrt{2x60x60x3.28x10^{-18}}$$

which is the correct order of magnitude considering the errors involved.

Calculations made from figure (35) indicate that the copper rich and copper impoverished regions are 35 A, and 25 A respectively. It would then appear that reprecipitation during fatigue at room temperature is both kinetically and thermodynamically feasible.

The specimen fatigued for 370,000 cycles shows a

further mode of precipitation, figures (42),(43). Measurements on the dark phase (spherical particles) indicate a mean diameter of 20-30 A. There are two feasible explanations which present themselves: an intermediate stage of reversion, or a further stage of precipitation.

A thin film of the 90,000 cycle specimen examined after one month at room temperature showed a precipitate, figure (37) which appears to be analogous. It is observed that both also show traces which are consistent with those of {110} planes. This would then discount the resolution hypothesis and it is concluded than some form of Ostwald Ripening effect is occurring on a very fine scale. This may be possible due to the high vacancy concentration and to the high degree of supersaturation involved.

#### CONCLUSIONS

- l/ Superston bronze does not exhibit spinodal decomposition. Instead, it would appear that a typical discontinuous eutectoid type of precipitation coupled with a very fine cubic semi-coherent precipitate enhance the mechanical properties in some undetermined manner.
- 2/ Oxygen present, even in small amounts (<300 ppm) destroys the ductility of the CuNiFe alloys. However, there is some anomaly present, since intergranular failure occurs only after ageing treatments within the miscibility gap.
- 3/ Maximum hardness, U.T.S. and elastic values at 640°C were attained after one to three hours; duration at temperature was not critical. The increase in these values was small, the greatest benefits being derived in elastic values. The optimum properties correspond to a modulation wavelength of roughly 220 A (this is not in agreement with the literature which generally cites values of 340-400A)
- 4/ The ageing sequence at 640°C appears to be as follows: semi-cubic spheres with a general trace consistent with {110} type planes linking together to form rods which in turm coarsen at the expense of their number and shape anisotropy. The linkage occurs at diameters of approximately 170 A. (This sequence is generally in agreement with Tufton

but at odds with the bulk of the literature. However the time sequence is much slower than that reported by Tufton)

- 5/ All of the CuNiFe alloys investigated gave very good fatigue ratios. Fatigue strengths at 10<sup>6</sup> both for annealed plus ageing and swaged plus ageing were roughly 40,000 psi. The best fatigue strengths reported for the Cu alloys seem to be found in the Cu-2%Be alloys, and the superston bronzes; both being of the order of 48,000 psi. However, it should be noted, that these values are reported for rotating bending which give values up to 20% higher than those found in direct stress (1). Thus, the fatigue strengths of the CuNiFe under rotating bending conditions may be as high as 45,000-49,000 psi at 10<sup>6</sup> cycles. This would then give fatigue ratios of approximately 0.6-0.65 which is considerably superior to any other Cu alloy.
- 6/ There is some indication that carbon bearing, oxygen free CuNiFe may realize greatly superior U.T.S. values than those found in this investigation (for carbon free material). Fatigue strengths may be also considerably higher, approaching those of the high alloy steels.
- 7/ The high Cu alloys of the CuNiFe series investigated exhibited appronounced discontinuity in the fatigue curves at 10<sup>4</sup>-10<sup>6</sup> cycles. There appears to be some correlation to the general notch sensitivity of the material ( the large grained annealed curve exhibiting the smallest discontinuity and the fine grained swaged material exhibiting the largest

discontinuity). The discontinuity could then be explained by an intrinsic variability in notch sensitivity caused by re-precipitation, as postulated by Mori (44), and Panseri (45): the re-precipitation phenomenon is observed by the author.

- 8/ CuNiFe is much less susceptible to varying grain size during fatigue than are most other copper alloys. (the fatigue ratios for 1.5 mm and 0.04 mm are 0.48 and 0.50 respectively)
- 9/ Examination of fatigued CuNiFe reveals that a reversion-reprecipitation-ageing process is occurfing. Calculations show that λ<sub>c</sub> at room temperature is 25-30 A and it is then postulated that relative displacement during fatigue "slices" the modulation until eventually the segments remaining are less than this value and thus redissolve. However, due to the great vacancy production, and to the thermodynamic implications of spinodal decomposition, re-precipitation occurs but on a much finer scale. This "new" modulation then ages during dynamic fatigue by some form of Ostwald Ripening effect.

### SUGGESTIONS FOR FUTURE WORK

This investigation indicates that very definite benefits can be derived from alloys exhibiting spinodal decomposition. More fundamental research should include:

- 1/ An examination of the intrinsic effects of oxygen and carbon on the mechanical properties of CuNiFe.
- 2/ A more thorough investigations into the effect of ageing treatment. (There is some indication of two hardening and U.T.S. peaks at 640°C; 1-3 hours, and 18-20 hours)
- 3/ An investigation determining the reasons for the observed discontinuities in the S. N. curves and the observed notch sensitivity correlation.
- 4/ A study of the slip formation on the surface during fatigue would either refute, or lend credence to the proposed localized slip hypothesis.
- 5/ A thorough investigation of the precipitation reversion and ageing effects observed during fatigue should include thin film work after relatively few cycles (100-1000 cycles) coupled with magnetic determinations during fatigue (the permeability will change as resolution or reversion occurs, thus allowing one to follow the ageing sequence during actual fatigue conditions)
- 6/ An investigation into the fatigue strengths at elevated temperatures. Values should be considerably higher

than those exhibited by nucleation and growth type alloys, due to the thermodynamic implications of spinodal decomposition.

7/ An investigation incorporating hysteresis measurements which could indicate the effects of wavelength and amplitude variation on the relative values of the elastic and frictional forces upon dislocations, and how they change during cycling.

#### REFERENCES

- 1. Forrest, "Metal Fatigue", Chapman and Hall (1959)
- 2. Templin, Proc. A.S.T.M., 54, (1954), 604.
- 3. Grover, "Fatigue of Metal", Thomson and Hudson, London (1956)
- 4. Orowan, Proc. Roy. Soc., A171, (1939), 79.
- 5. Thompson, Adv. Phy., 7, (1958), 72.
- 6. Kennedy, "Proc. of Creep and Fatigue in Metals," Oliver and Boyd, Edinburough and London, (1962)
- 7. Broom et al, J.I.M., 86, (1957), 17.
- 8. McEvily et al, Trans. A.I.M.E., <u>227</u>, (1963), 1093.
- 9. Hanstock, J.I.M., 83, (1954), 11.
- 10. Clark and McEvily, Acta Met., 12, (1964), 1359.
- ll. Coffin and Tavernelli, Trans. A.I.M.E., 215, (1959), 794.
- 12. Abel and Ham. M.Sc. thesis. McMaster. (1965)
- 13. Burghoff and Blank, Proc. A.S.T.M., 48, (1948), 709
- 14. Gibbs, Collected Works, Yale University Press, (1948)
- 15. Koster et al, Z. Metallk., 29, (1935), 173.
- 16. Bradley et al, J.I.M., 67, (1941), 189.
- 17. Daniel and Lipson, Proc. Roy. Soc., A182, (1943), 368
  A181, (1941), 378
  A192, (1948), 579
- 18. Becker, Z. Metallk., 29, (1951), 301.
- 19. Hargreaves, Acta Crys., 4, (1951), 243.
- 20. Balli and Zakharova, Doklady Akad. Naut., U.S.S.R.
- 22. Tiedema, Bouman and Burgers, Acta Met., 5, (1957), 310.

- 23. Geisler, Trans. A.S.T.M., 43, (1951), 70.
- 24. Hibbard, Jour. of Met., 8, (1956), 862.
- 24. Sucksmith, E.R.A. Rep. N/C/T26, (1945)
- 26. Arndt, PhD Thesis, Cambridge University, (1948)
- 27. Biedermann and Kneller, Z. Metallk., 47, (1956), 289.
- 28. Bailey, J.I.M., 79, (1951), 243.
- 29. Pines and Barutkin, Fiz. Met., 6, (1958), 96.
- 30. Geisler, Trans. A.S.T.M., 43, (1951), 77.
- 31. Guinier, Acta Met., 3, (1955), 510.
- 32. Z. Becker, Z. Metalik., 29, (1937), 243.
- 33. Borelius, Trans. A.I.M.M.E., 191, (1951), 477.
- 34. Hillert, Acta. Met., 9, (1961), 525.
- 35. Hillert, Cohen and Averbach, Acta Met. 9, (1961),536.
- 36. Cahn, Acta Met., 9, (1961), 795.
- 37. Cahn and Hilliard, J. Chem. Phy. 28, (1958), 256.
- 38. Cahn, Acta Met., 10, (1962), 179.
- 39. Cahn, G.E. Rep. 63 RL 3256 M, (1963)
- 40. Tufton, PhD. Thesis, Cambridge University (1963)
- 41. Barrett, "Structure of Metals" McGraw-Hill, (1952)
- 42. Burgess and Aston, Jour. Met. and Chem. Eng., 8, (1910), 452.
- 43. Clamer, Jour. Met. and Chem. Eng., 8, (1910), 527.
- 44. Mori, Istituto Sperimentale dii Metalli Leggeri (Milan), 270, (1961)
- 45. Panseri et al, ibid., 270, (1961)

- 46. Finney, J.I.M., 92, (1964), 580.
- 47. Oding, Doklady Akad. Nauk. S.S.S.A., <u>105</u>, (1955), 1238.
- 48. Shabalin, ibid, 122, (1958), 600.
- 49. Karry and Dolan, "Influence of Grain Size on Notch Sensitivity", Proc. A.S.T.M., 53, (1953), 789.
- 50. Massonnet, Proc. A.S.T.M., <u>56</u>, (1956), 954.
- 51. Cook and Hilliard, Trans. A.I.M.E., 233, (1965),142.
- 52. M. Wayman, Continuous Spark Cutter, McMaster.
- 53. Seitz, Adv. Phys., 1, (1952), 43.
- 54. Mott, Phil. Mag., <u>43</u>, (1952), 1151; ibid, <u>44</u>, (1953), 187, 742.
- 55. Coffin, G.E. Res. Lab. Reprint 61-WA-199 (1962)
- 56. Smithells Metals Referance, volume 2
- 57. Panseri, et al, Allumino, 28, (1959), 113.
- 58. Wilkens, Gough and Sopwith, J.I.M., 60, (1937), 143
- 59. Private communications, Black, Clawson-Kennedy Ltd.
- 60. Private communications, Canaidian Copper and Brass Association, Toronto-refer to publication CDA 54
- 61. Burghoff and Blank, Proc. A.S.T.M., 48, (1948), 709
- 62. Sinclair and Craig,, Trans. Amer. Soc. Mat., <u>44</u>, (1952), 929
- 63. Anderson et al, Proc. A.S.T.M., 46, (1946), 678

### APPENDIX A

## Alloy Preparation

Initially, 30 pound heats of CuNiFe (heats 1,2) were prepared in a vacuum induction unit furnished by Falconbridge Nickel Mines of Toronto. The material was deoxidized with two different levels of graphite, and cast in vacuum at 1500°C into zircon sand molding. Considerable pipe formed on cooling (indicating an unusually high coefficient of expansion) and only 10 pounds of material could be salvaged. The cropped ingots were homogenized at 1050°C for 10 hours and extruded (20/1) to 0.75" diameter rod at the Dept. Mines and Technical Surveys.

Sixty pounds of 60/20/20-Cu/Ni/Fe was also purchased from Indiana Steel Co., Valparaiso, Indiana in the as cast condition.

Both materials after subsequent heat treatment within the miscibility gap were found to fail intergranularly in tension. Thin films were prepared, but showed no intergranular precipitation to be present, even at the highest magnifications (100,000%). It was concluded that either carbon, and/or oxygen were causing this failure in some undetermined manner.

It then appeared that the problem lay not in the alloy preparation, but in the subsequent forming at red heats in air (oxygen diffusion) which was necessary to

to obtain the material in the desired shape for swaging. Casting under vacuum also would not be satisfactory due to the excessive pipe formation rendering a great proportion of the heat useless.

It was thus necessary to devise a technique in which bulk material could be induction melted (ensuring good homogenization) and cast in the form of rods and then rapidly quenched such that pipe formation could be restricted.

Refer to figure 2. It was found that by sucking material up vycor tubing from the melt, the top would freeze and the bottom, still remaining in the melt, would restrict pipe to small values (if the correct tubing diameters and preheats were chosen)

Optimum diameters and preheats were critical,

0.1"-0.6" and 50-100°C giving good results. Recrystallized alumina crucibles 2 " in diameter by 4" in height were chosen. These in turn were packed with kyanex in a quartz tube 6" by 75 mm diameter, one end being plugged for support. This assemblage was baked at 150°C/10 hours to dry off excess water, and harden the complete unit. The complete crucible unit and manifold assembly was, in turn, enclosed in a 3 ft. by 90 mm pyrex tube plugged at each end, with provisions for Argon entry and exit.

The Argon was passed through a standard purificat-

son unit ( Ascarite/CO<sub>2</sub>, MgClO<sub>4</sub>/H<sub>2</sub>O<sub>v</sub>, Activated Cu/O<sub>2</sub> ) and then flushed through the unit.

to cool the pyrex in the vicinity of the molten heat. When the charge is fully molten and sufficient time has been allowed for complete stirring to occur, the overall manifold assemblage is introduced into the melt. Since the vacuum pump is creating a pressure drop, the molten material is sucked up the four vycor tubes simultaneously. If the tube diameter and the preheat are correctly chosen, the columns will rise 12-15" before the top freezes. Just before the overall remaining melt in the crucible freezes, the complete manifold assemblage is removed and quenched in water. The enclosed cast rods should then drop out off the vycor tubes thus allowing the unit to be reused.

Four pound heats of Cu rich, Ni rich, and Fe rich CuNiFe, two pound heats of Cu-2%, Cu-4% Co, and a 100 gram heat of superston bronze were successfully prepared in this manner. A heat of Cu rich CuNiFe was half drawn, and the remaining portion was deoxidized with 0.01% Al to investigate oxygen pickup. Subsequent tensile tests showed no significant difference.

Excellent cleanliness combined with low porosity and very good cast surface could be expected. The cast material was then swaged at room temperature down to the desired diameters (no annealing treatment was required)

### APPENDIX B

## Calibration of Fatigue Machine

It was decided that for meaningful fatigue results, dynamic load calibration was necessary, as the Baldwin Sonntag had not been checked for over four years.

Previously, strain gages had been incorporated but it was found that conflicting results occured and the technique was very involved. Several different methods were investigated, two of which shall be summarized.

The first method which showed some success involved a photostress plastic (Budd Instruments Ltd.) mounted on a fatigue specimen. This material, under an applied stress shows fringes when viewed under polarized light. The shift of fringes can be calibrated to a change of dead weight load. Under dynamic conditions, a stroboscope is employed thus effectively "stopping" the fringe. However, the fatigue machine does not operate exactly at the resonant frequency it was designed for, and as a result, fluctuates slowly about the main resonant frequency. To correct for this, it is necessary to dynamically readjust the strobe frequency with a slip-synch unit, which effectively changes the flashing frequency of the strobe to exactly match the changing resonant frequency. By this time, however the overall test unit is self-defeating, as the inaccuracy of

of the electronics so-involved is of the order of 5%. It was estimated that the overall efficiency of the unit was 10%, but was inaccurate below dynamic loads of 200 pounds.

The second method was very simple, and gave very good calibration, to ±1% applied load (either dynamic or static); it was also possible to readjust under dynamic conditions for equal tensile and compressive half cycles to ±1% applied load.

It was discovered that a differential transformer is incorporated on the Baldwin which is employed as an automatic regulating device for creep during fatigue. This could be easily reconnected for calibration measurements. The differential transformer is a device in which a primary signal at a fixed frequency and potential difference is imposed across the primary coil. Since the potential difference across the secondary coil is a function of the magnetic coupling efficiency, and change in the relative position of the ferrite core will influence this relative efficiency, then any displacement will affect the secondary potential difference. The coils are contained in a plastic core mounted on the fixed frame of the fatigue machine, whereas the ferrite core is attached to the moving frame. Thus any displacement of the moving grame can be followed by a change in the potential difference developed across the secondary coil.

For the calibration, a 2000 cycle stabilized sig-

nal was imposed across the primary and dead weights were placed on the moving frame. The secondary potential was connected to a high gain stabilized oscilloscope (provided by Dr. M. B. Ives) and recorded by a cathetometer. Peak heights were then recorded for different dead weights and a plot of dead weight versus cathetometer reading was made. In the same way, a plot of dynamic load versus cathetometer reading was made and a third plot (fig.3) of dead weight versus dynamic weight could then be constructed.

## APPENDIX C

## Electron Microscopy

Direct observation of CuNiFe by transmission electron microscopy has been restricted in the past due to inadequate polishing techniques. Tufton (40) summarized solutions with which he obtained partial results.

All electropolishing techniques that he considered involved the formation of a film by some corrosiMe chemical agent and the removal of it by an electrochemical action; unfortunately, CuNiFe gave an exceedingly tenacious film. It would appear that a complex oxide was formed which only is selectively removed at low current densities leaving a black insoluble film. At high current densities, it was completely stripped off, but severe pitting took place producing wedge shaped films which were thin enough for transmission only at the extreme edges.

The polishing solutions depend on the thickness of the polishing layer which impedes ionization but is essential for a smooth finish, and as the layer flows downwards under the influence of gravity it builds up significantly thicker and as a result preferential thinning occurs at the top of the film. It was found by this author that surface contamination also was occurring as eximplified by spotty diffraction patterns being observed.

Various solutions were then investigated and it was found that a modified Nitric acid/Methyl Alcohol mixture gave excellent results. In addition, the solution polished Superston bronze, and copper-cobalt with equal ease.

The system polished by a gaseous evolution at the specimen surface, and thus the ionization impediment is towards the upper half of the foil, resulting in preferential polishing at the bottom of the foil. However, if conditions are correct, the insoluble oxide formation can be completely removed resulting in clean foil surfaces.

If the following procedure is followed, good results may be obtained. The material to be examined is rolled down to strip 5-20 mils thick (the thinner the better). After the desired heat treatments, an extremely tenacious oxide layer forms which is removed by 600 grit paper. It is important that this is removed prior to polishing for satisfactory results to be obtained. The polishing solution can be 60-80% Methyl Alcohol (the higher percentage for higher copper contents). The solution is cooled to -40 C < T < -20 C. The clean foils are cut to approximately 1 cm and microstopped about the edges. The specimen is then introduced into the solution; stainless steel cathodes and voltages of 6-10 volts gave optimum results.

The optimum voltage appears to be dependent on the foil size; 10 volts for foils 2 cm by 1 cm, and 6 volts for foils 0.1" in diameter. A good indication of the correct voltage (which is critical for uniformly thin foils) is the specimen surface during polishing. With voltage at zero and specimen immersed, increase the voltage until vigorous bubble evolution occurs, then decrease voltage until bubbles are just being produced at the surface; the latter voltage will be lower than that to produce initial evolution (due probably to activation polarization effects) and is the correct one. During polishing, it is important that the specimen or solution not be agitated. However, the specimen should be rotated 180 for a predetermined length of time and then rotated back to its original position. This is repeated until the foil goes through somewhere across the middle diameter, usually at the edge. The specimen is then rotated 90° such that the hole so produced is now at the top when immersed again. The foil is introduced and will go through at the bottom almost immediately, and the two holes will grow together. Remove the finished foil and quickly introduce it into a clean solution of ethyl alcohol cooled to approximately -40 C and rapidly agitate (polishing solution will etch the thin film very rapidly). Incorporating this technique will produce 2-3 good films from each initial foil.

After the desired heat treatments, the fatigue specimens were ground to the desired shape and were then electropolished. Technique was not as stringent as previously outlined; temperatures up to -10 C could be tolerated. If a black deposit begins to form on the specimen during polishing, the solution must be renewed. (200 ml will polish 5 specimens)

Table 1

Material	Condition	Tensile Strength (tons/in <sup>2</sup> )	Fatigue Strength 10 <sup>6</sup> /R.B. (tons/in <sup>2</sup> )
Cu	Drawn 30%	19.6	11.2
70/30-Cu/Zn	" 21%	25•4	14.0
60/40-Cu/Zn	" 24%	38.8	21.4
87/10/2- Cu/Al/Fe	" 10%	41.4	20.6
68/31 <b>-</b> Cu/Ni	" 33%	36.4	19.1
95/4.5/0.5- Cu/Sn/P	" 50%	43.1	19.2
97/1.5/1.5- Cu/Si/Zn	<b>-</b>	41.7	20.6
98/2 <b>-</b> Cu/ <b>Be</b>	Drawn fully hard plus Prec. hardened	89.5	16,6/ 10 <sup>8</sup> cyc- les

Table 2

Heat	Treatment	Elastic Limit p.s.i.	U.T.S. p.s.i.	Fracture
I	*	35,000	86,000	d,t
	*+580°C/52 hrs.	55,000	100,000	b,i
	*+730°C/4 min.	40,000	88,000	b,i
2	extruded normalized	91,000	150,000	b,t
	*+580°C/66 hrs.	90,000	142,000	b,i
	1) *+825°C/2 2) min.	-	83,000	d,t
	1) *+810°C/5 2) min.	-	88,000	b, <b>i</b>
	1) as swaged 2) cold	-	122,000	đ,i
	1) * 2)	-	78,000	đ,t
	1) *+710°C/1 2) min.	-	86,000	d,t
	1) *+710°C/5 2) min.	-	97,000	b,1
6	2) *	47,800	86,000	vd,t
	2) ***630°C/l hr.	52,500	92,500	vd,t
	2) *-630°C/1.5 hrs.	53,000	93,000	vd,t

Heat	Treatment	Elastic Limit	U.T.S.	Fracture
		p.s.i.	p.s.i.	
6	2) *+630°c/ 4 hrs.	54,400	88,500	vd,t
	2) *+630°C/ 8 hrs.	-	86,000	d,t
	2) *+630°C/ 15 hrs.	55,500	84,800	d,t
	2) ***630°C/ 27 hrs.	-	87,000	d,t
	2) as swaged	92,000	101,000	đ,t
4	2) *	36,800	67,000	d,t
:	2) *+640°c/ l hr.	46,000	75,200	d,t
	2) *~640°C/ 4 hr.	44,000	70,200	d,t
	2) *+640°C/ 8 hr.	39,000	56,000	d,t
	2) **640°C/ 15 hr.	35,000	58,000	d,t
	2) as swaged	60,000	70,000	vd,t
	3) *+640°C/ 2 hr.	These spe	cimans showed	porosity
5	Annealed 880 °C 7 640°C/2 hr.		31,000	vd,t
7	*+640°C/2 hr.	52,500	76,500	d,t
	swaged > 640°C/ 2 hr.	76,500	91,000	d,t

Heat	Treatment	Elastic Limit p.s.i.	U.T.S. p.s.i.	Fracture
8	2) *	49,700	69,000	d,t
	2) swaged	95,000	119,000	d,t
	2) #+640°C/ l hr.	46,000	76,600	d,t
	2) *+640°c/ 3 hr.	56,000	82,500	d,t
	2) *+640°C/ 8 hr.	47 <b>,</b> 500	81,000	d,t
	2) *+640°c/ 15 hr.	45,000	78,000	đ,t
9	2) *	37,000	80,000	d,t
	2) swaged	94,000	110,000	d,t
	2) *+640°c/ 3 hr.	52,000	76,000	d,t

<sup>\* --</sup> Annealed at 1850°F 1-2 hours.

2) -- Swaged from 0.4" to 0.1" cold without intermediate heat treatment.

b--- brittle failure

d--- ductile fracture

vd-- very ductile

i--- intergranular failure

t--- transgranular failure

<sup>1) --</sup> Tensile tests performed on Hounsfield

Table 3

Heat	%Cu	%Ni	%Fe	%Co	%A1	C ppm	O mgg	Grain Size
1	53.6	32.2	14.2	-	-	20 to 1000	-	0.5 mm
2	55•4	31.1	13.5	-	-	60	343	0.05 mm
3	80	5	5	-	10	-	-	-
4	96	-	-	4	_	-	-	0.03 mm
5	98	-	_	2	-	-	-	1.5 mm
6	66.3	19.2	14.5	-	-		<b>-</b>	1.5
7	65.4	17.3	17.3	-	_	31	80	0.04 mm
8	10.6	24.6	64.8	-	-	_	-	0.06 mm
9	21.2	40.8	38.0	-	_	<u>-</u>	<u>-</u>	0.05 mm

Table 4

Heat	Dynamic Stress p.s.i.	Number of Cycles to Failure	Fatigue Ratio at 10 <sup>6</sup> Cycles
5	17,000	18,000	
	15,000	106,000	
	13,300	252,000	0.36
	11,800	435,000	
	11,400	1,512,000	
6	48,700	1,000	
Annealed	41,000	21,000	
+ Ageing	37,000	53,000	
	35,500	211,000	0.48
	35,500	310,000	
	33,000	723,000	
	32,500	1,634,000	
6	34,500	1,000	
Annealed	27,500	82,000	
	23,600	311,000	0.41
	23,000	540,000	<b>3</b> € ₹ ±
	22,800	764,000	
	22,000	1,181,000	

Heat	Dynamic Stress p.s.i.	Number of Cycles to Failure	Fatigue Ratio at 10 <sup>6</sup> Cycles
7	52,500	24,000	
Annealed	48,000	44,000	
Ageing	42,000	105,000	
: :	41,000	219,000	0.50
	40,000	403,000	
	39,500	532,000	
	39,200	1,056,000	
7			
Swaged	57,500	11,000	
Ageing	50,500	102,000	
	48,500	190,000	
İ	46,000	325,000	
	44,200	328,000	0.43
	43,000	375,000	
	40,000	446,000	
	39,600	582,000	
	37 <b>;5</b> 00	2,852,000	

Heat	Dynamic Stress p.s.i.	Number of Cycles to Failure	Fatigue Ratio at 10 <sup>6</sup> Cycles
8	44,400	9,000	
	43,000	31,000	
	40,000	84,000	
	39,000	183,000	0.53
	39,000	410,000	
	37,900	1,257,000	
	37,600	2,334,000	
9	54,000	2,000	
	42,500	76,000	
	41,000	210,000	0.50
	39,800	870,000	
	37,000	2,134,000	

`

Table 5

Author	Alloy	U.T.S. p.s.i.	Fatigue Strength p.s.i. *	Fatigue Ratio
(57)	(1)	128,000	55,000/10 <sup>6</sup>	0.43
	(2)	109,000	38,300/10 <sup>6</sup>	0.35
	<del></del>		. 7	
(58)	(3)	116,000	51,000/10 <sup>7</sup>	
(59)	(4)	110,000	42,000/10 <sup>8</sup>	

## \*--Rotating beam

- (1)-Xantal B (Cu/Al/Fe/Ni-81/10/4/4 %), 890°C/2 hours 620°C/1 hour.
- (2)-Xantal M (Cu/Al/Mn/Ni/Fe/-75/8/11/2/2 %), 850°C/2 hours 600°C/1 hour.
- (3) (Cu/A1/N1/Fe-80/10/5/5%), hot forged.
- (4) Superston Seventy, (Cu/Mn/Al/Ni/Fe-60/30/8/1/1 %) furnace cooled at 7°C/hour.

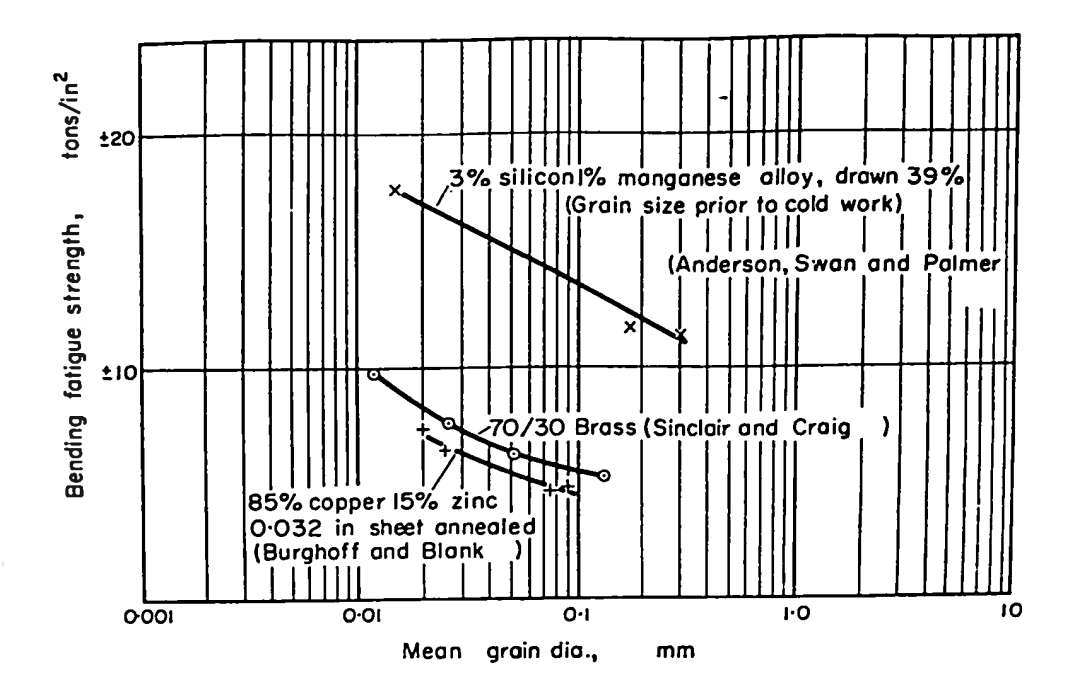


Fig. 1 Effect of grain size on fatigue strength.

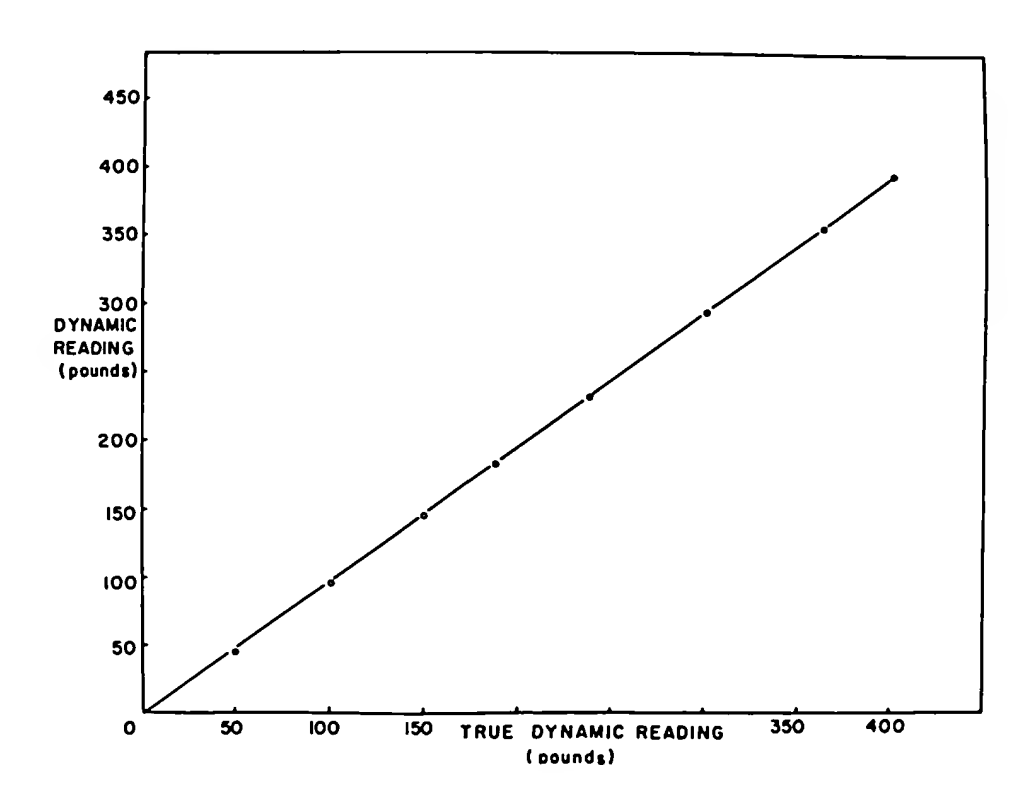


Fig. 3 Calibration plot for fatigue machine.

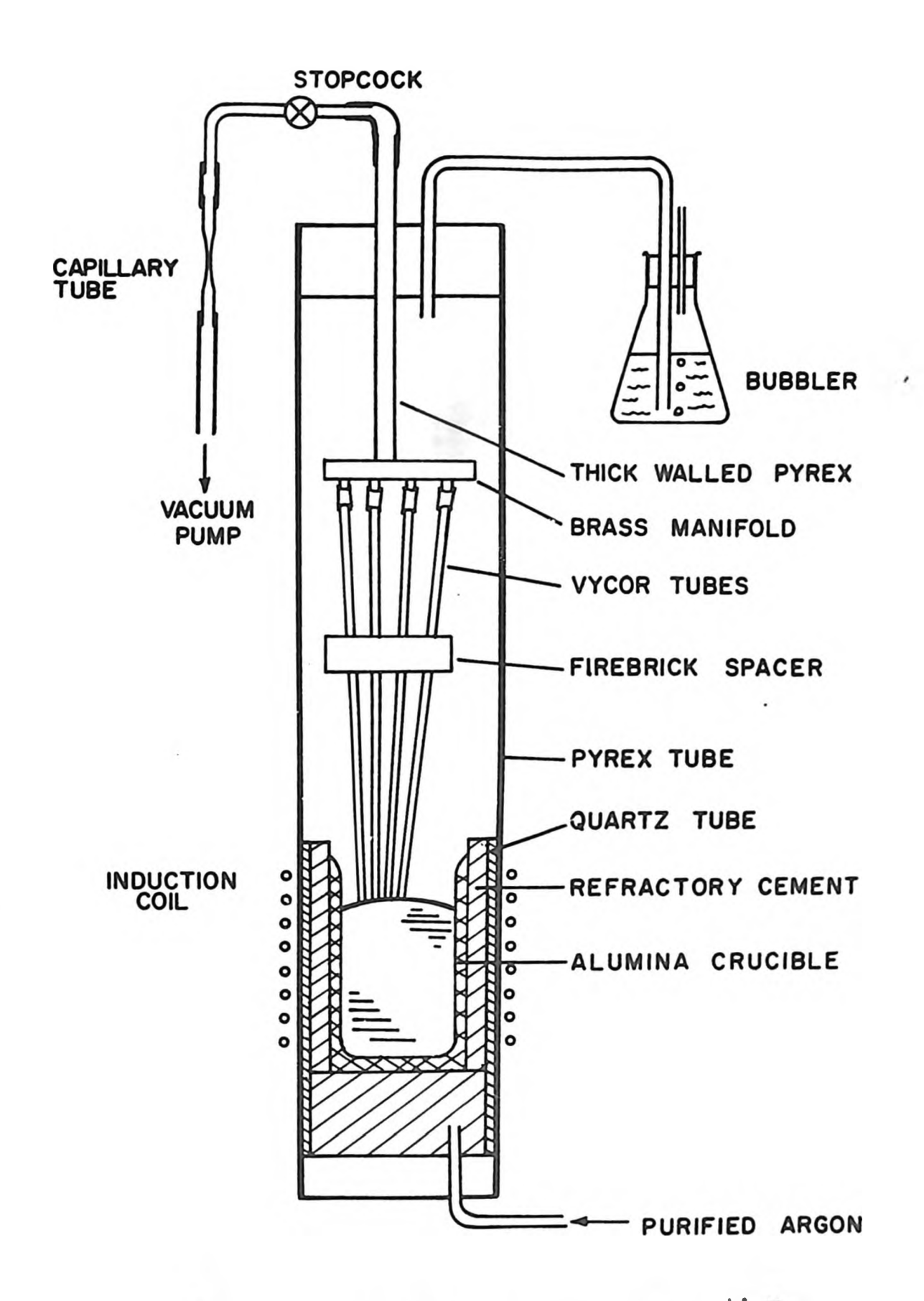


Fig. 2 Apparatus for alloy preparation.

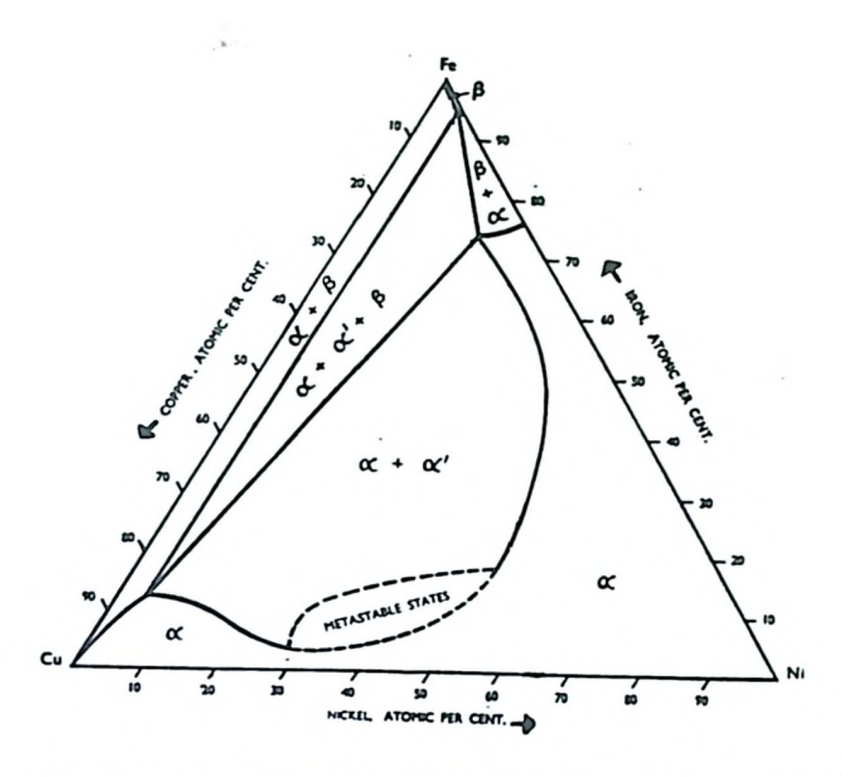


Fig. 4 Phase diagram for Cultire (slow cooled)



Fig. 5 Superston bronse, typical structure for both heat treatments. 16000



Fig. 6 Slow cooled Superston Bronze, coarsening of random lamellae. N3,500



Fig. 7 Diffraction pattern of dark lamellae in figure 6. (foil normal [111])



Fig. 8 Diffraction pattern of matrix in figure 6 (foil normal [121])



Fig. 9 Cubic precipitates, slow cooled Superston Bronze. X104,000

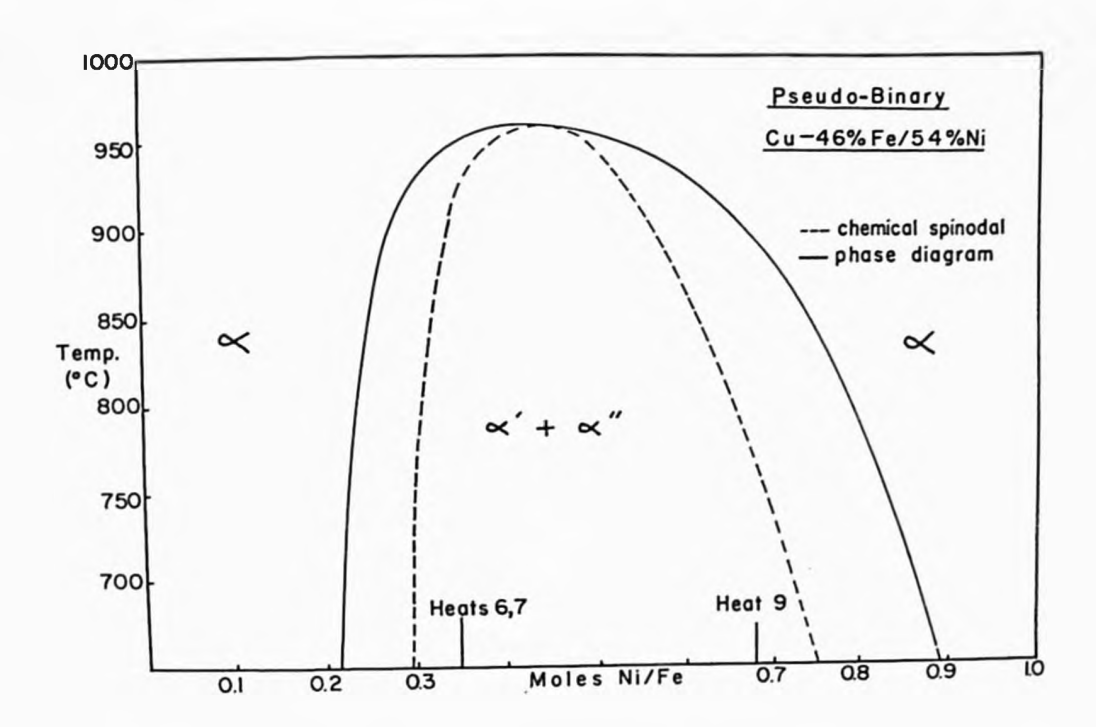


Fig. 10. Pseudo-binary calculated as in (16,51)

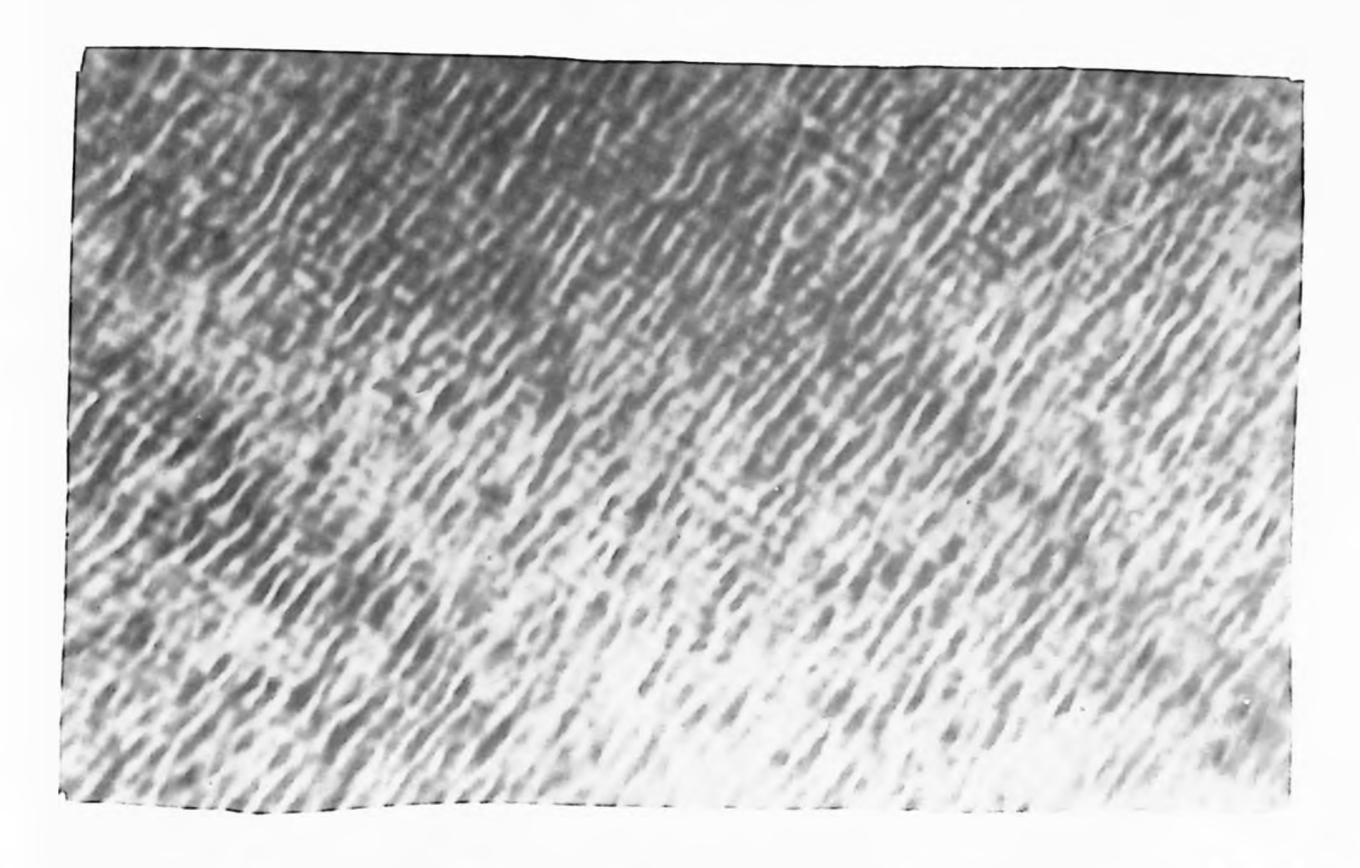


Fig. 11. Typical modulation observed, traces {110}. X80,000

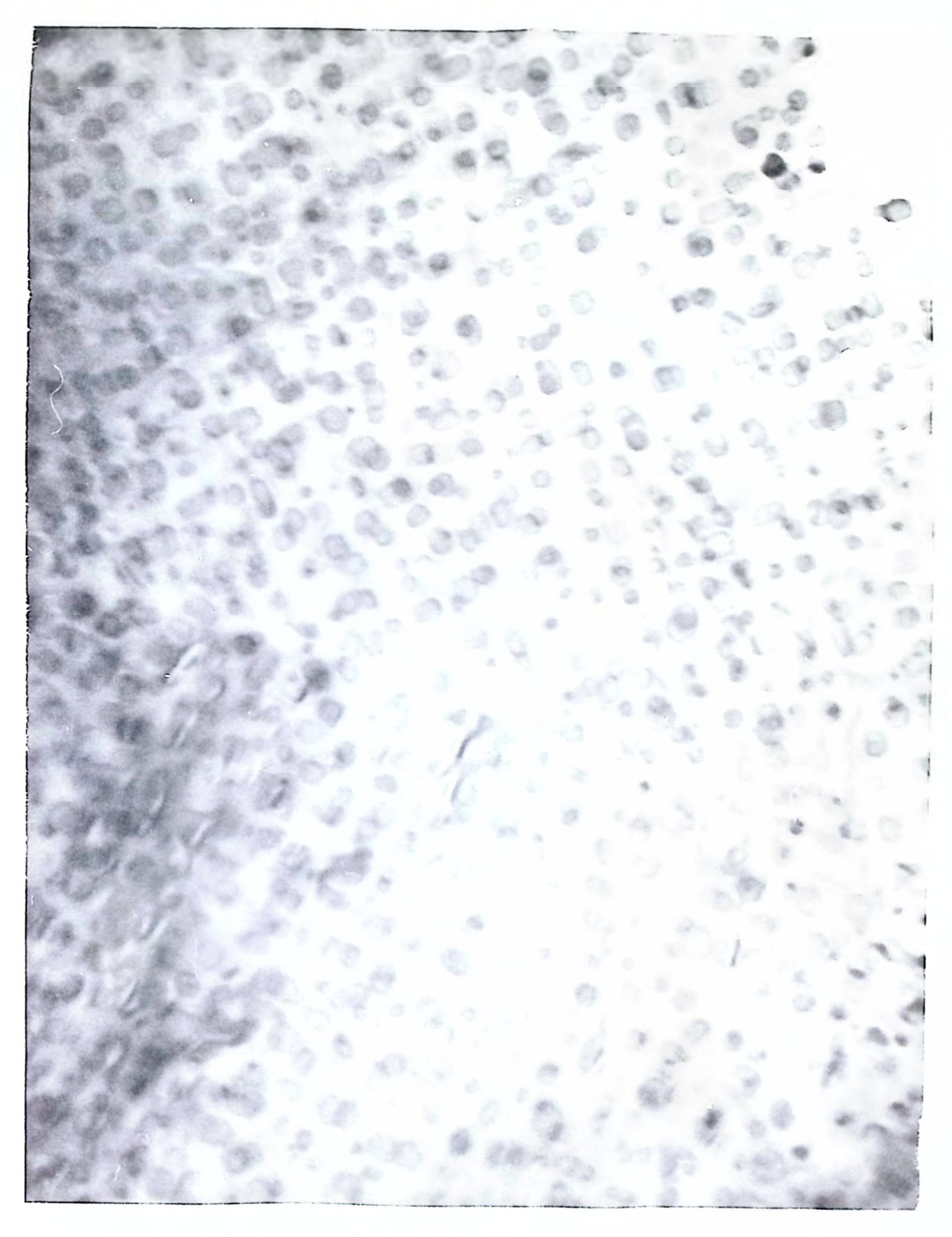


Fig. 12 Precipitate after 60 minutes at 640°C (heat 7). X215,000

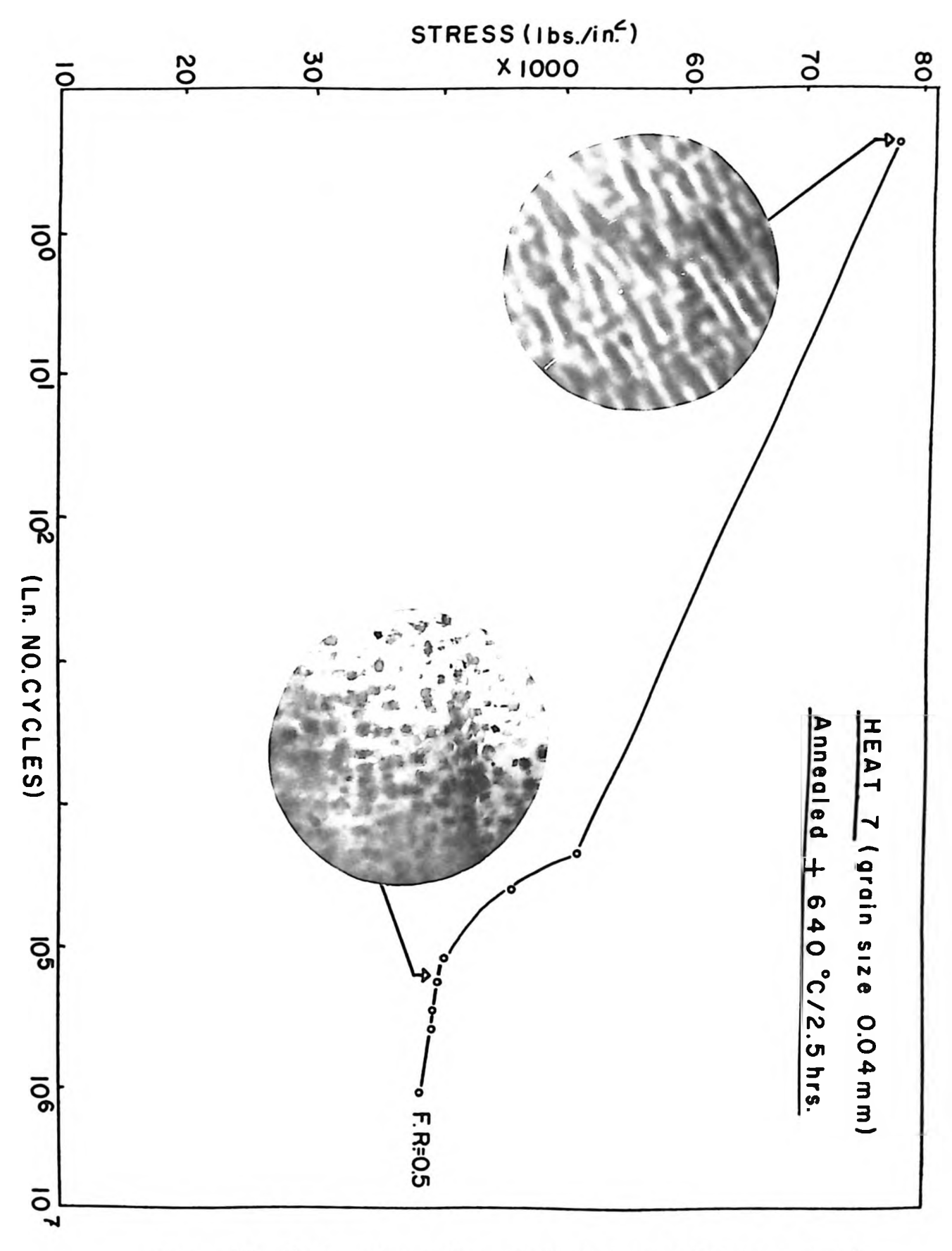
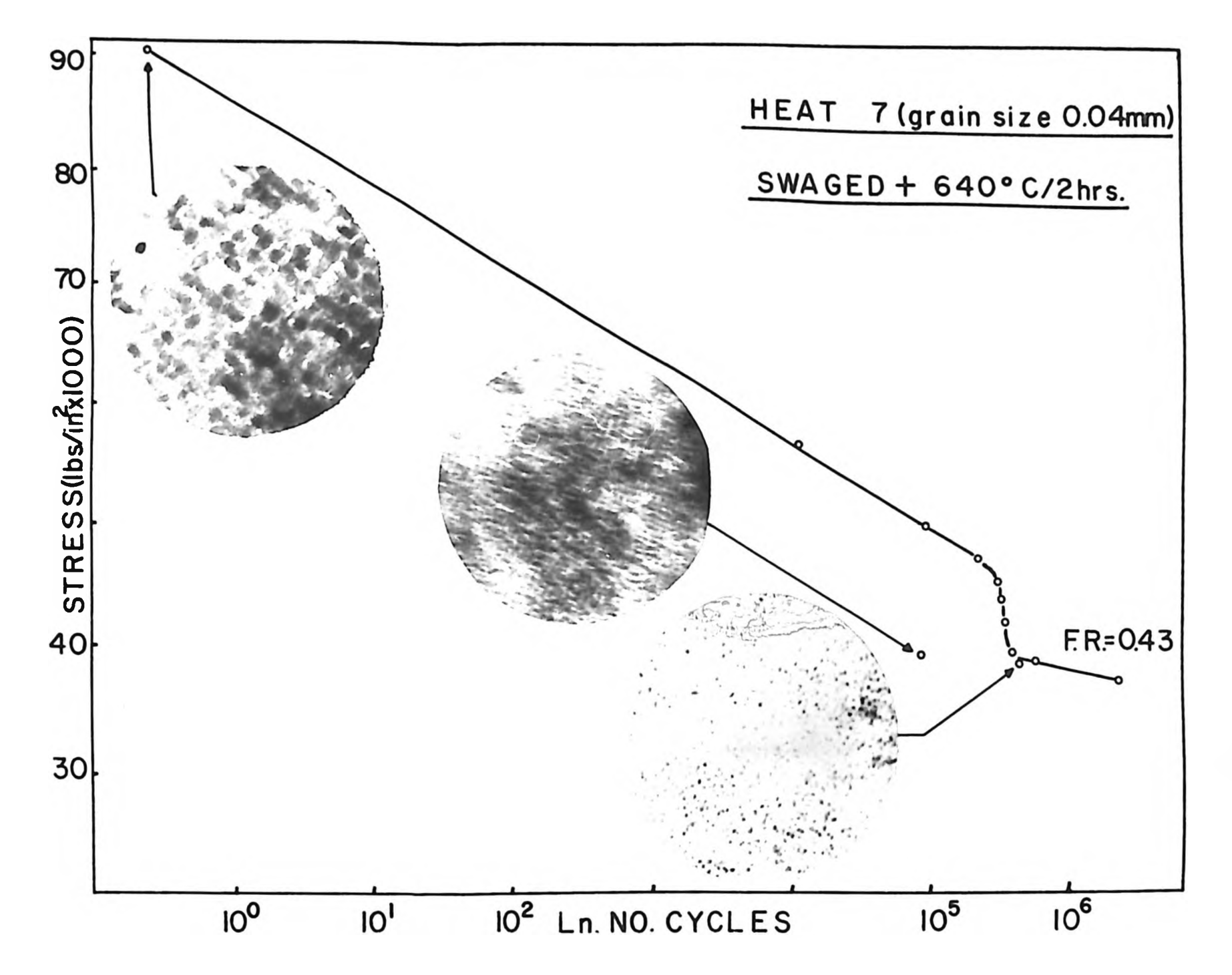


Fig. 14 S.N. curve for heat 7 (annealed + ageing)



S.N. curve for heat 7 (swaged+ ageing) Fig. 15.

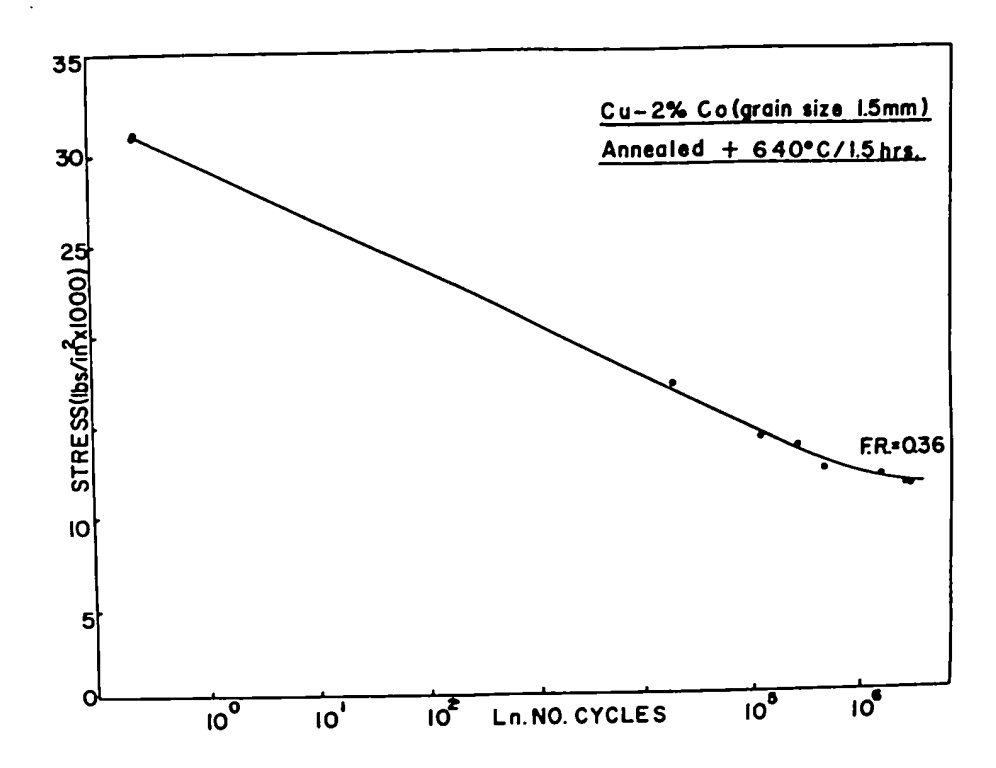


Fig. 16 S.N. curve for heat 5.

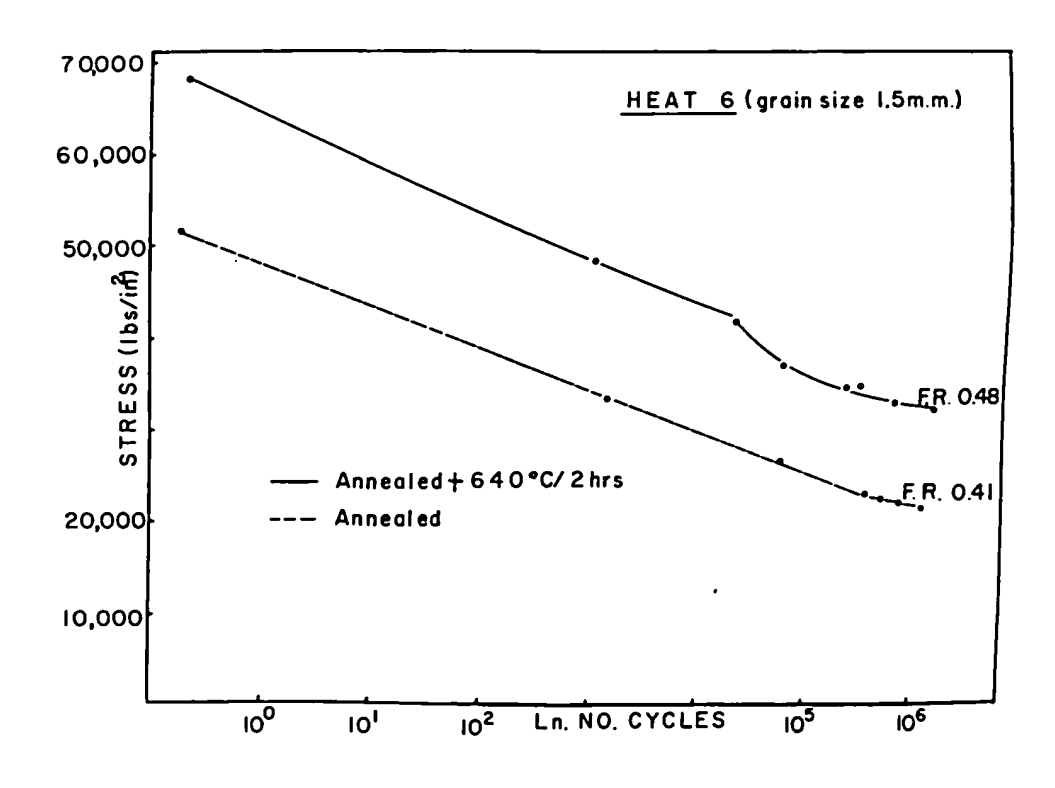


Fig. 13 S.N. curve for heat 6.

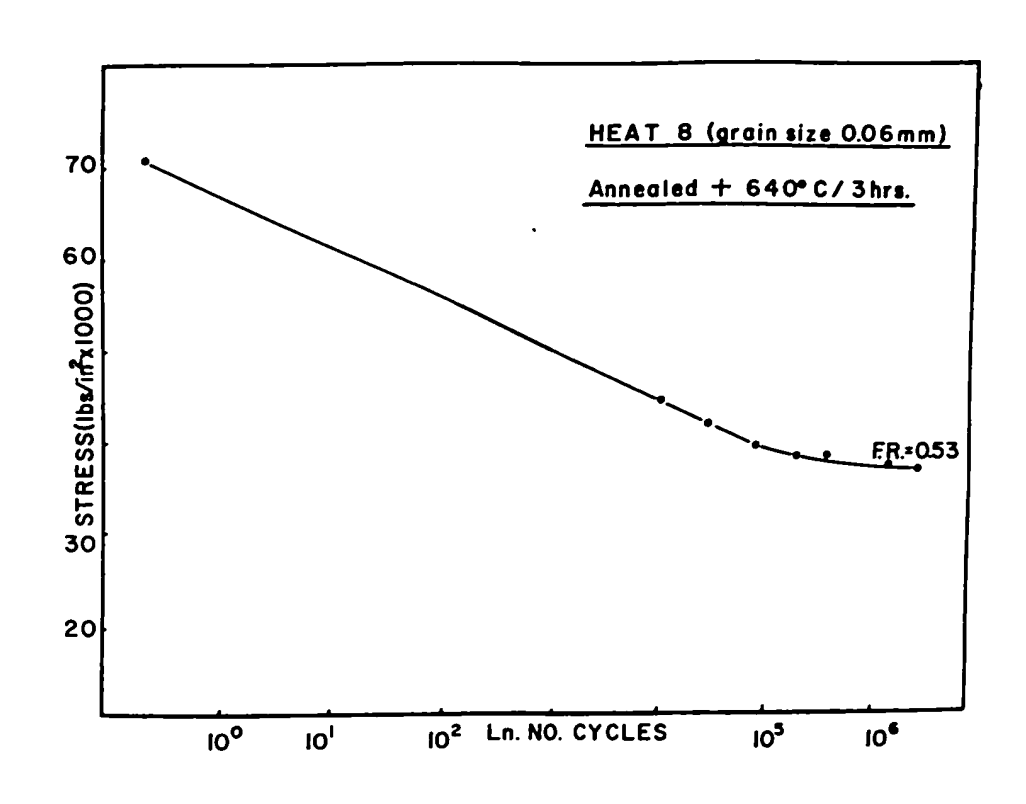


Fig. 17 S.N. curve for heat 8.

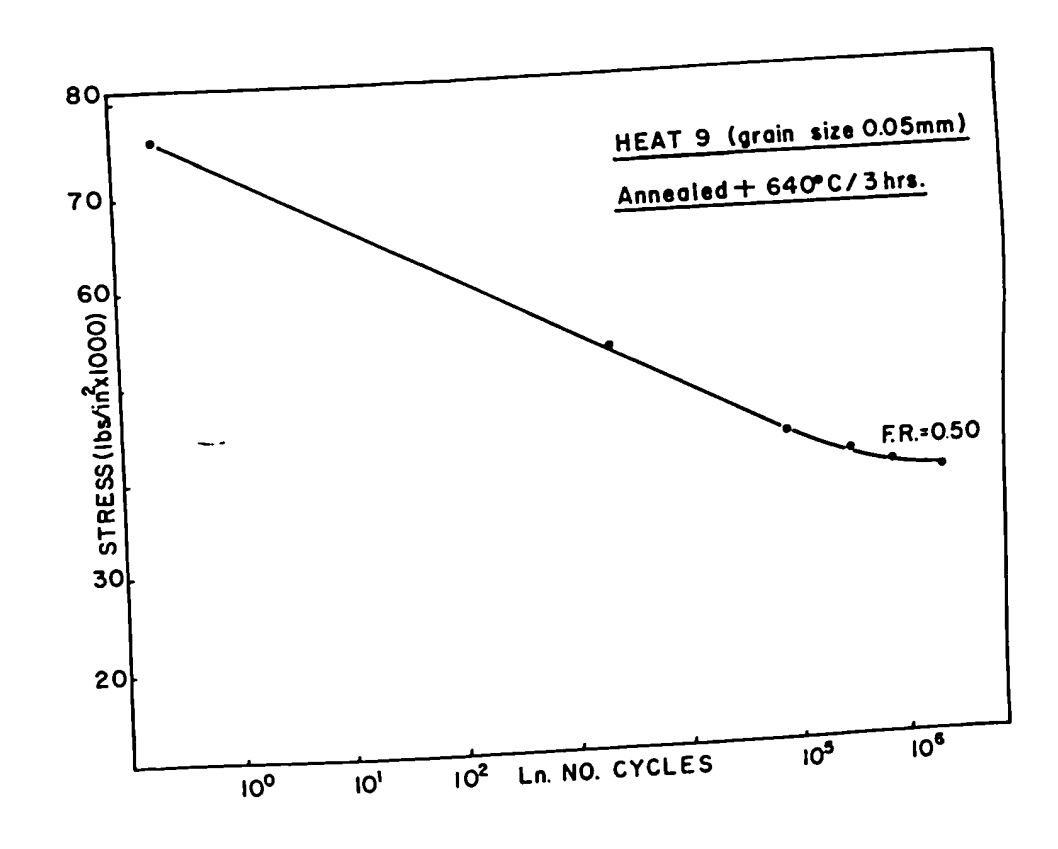


Fig. 18. S.N. curve for heat 9.

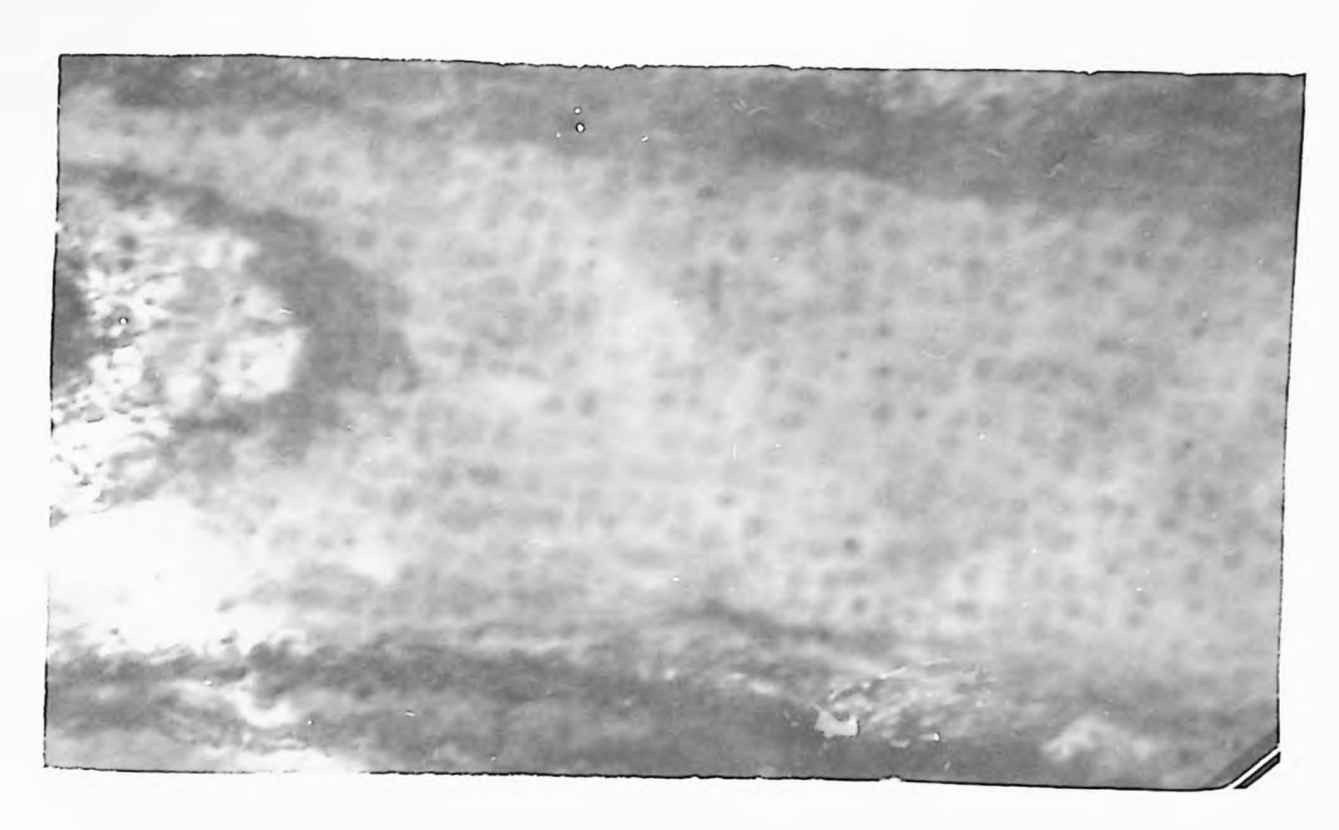


Fig. 19 Microstructure after fatigue, diffraction effect. X66,000



Fig. 20 Microstructure after fatigue, diffraction effect. X152,000

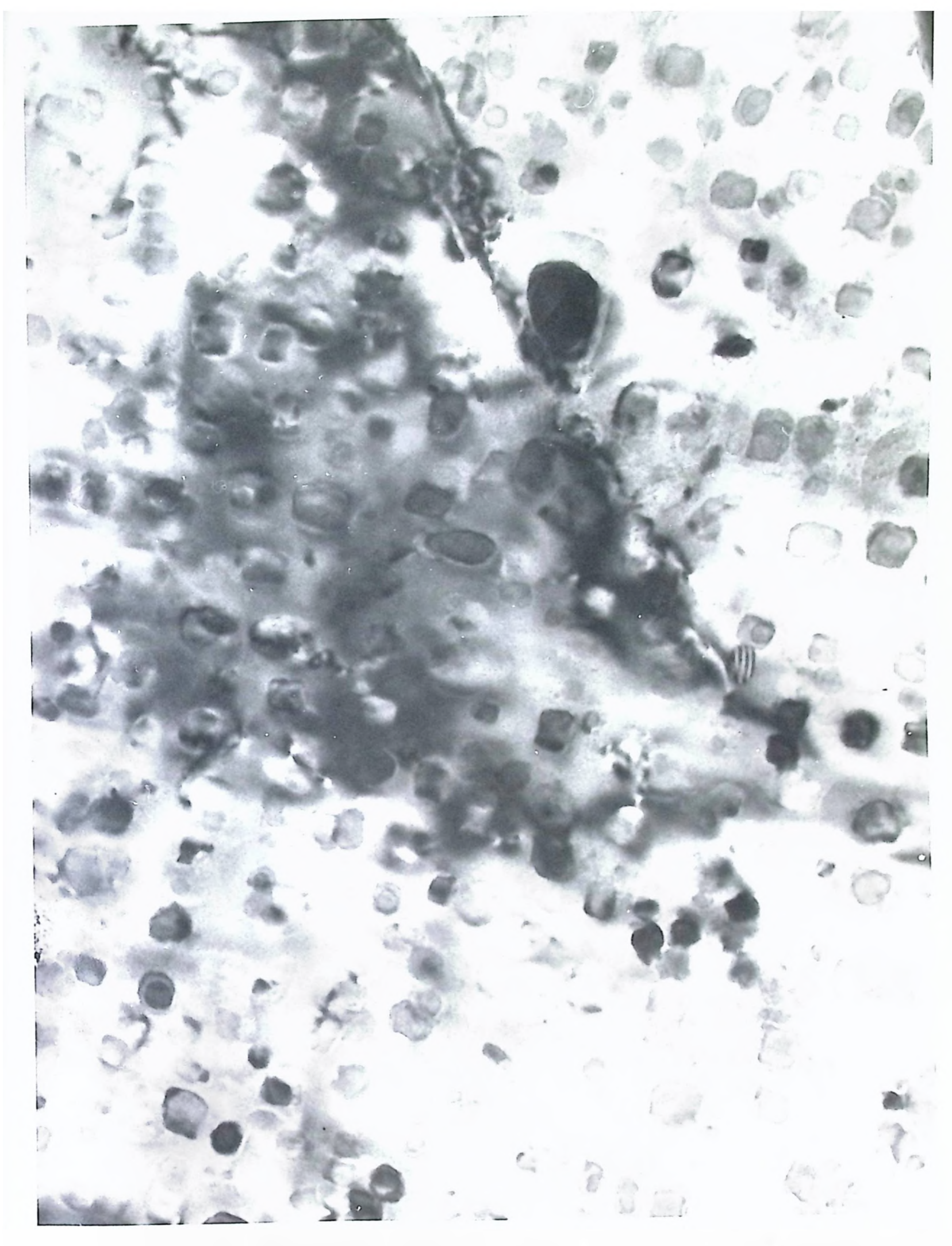


Fig. 22 Patigued structure, diffraction effect. X315,000

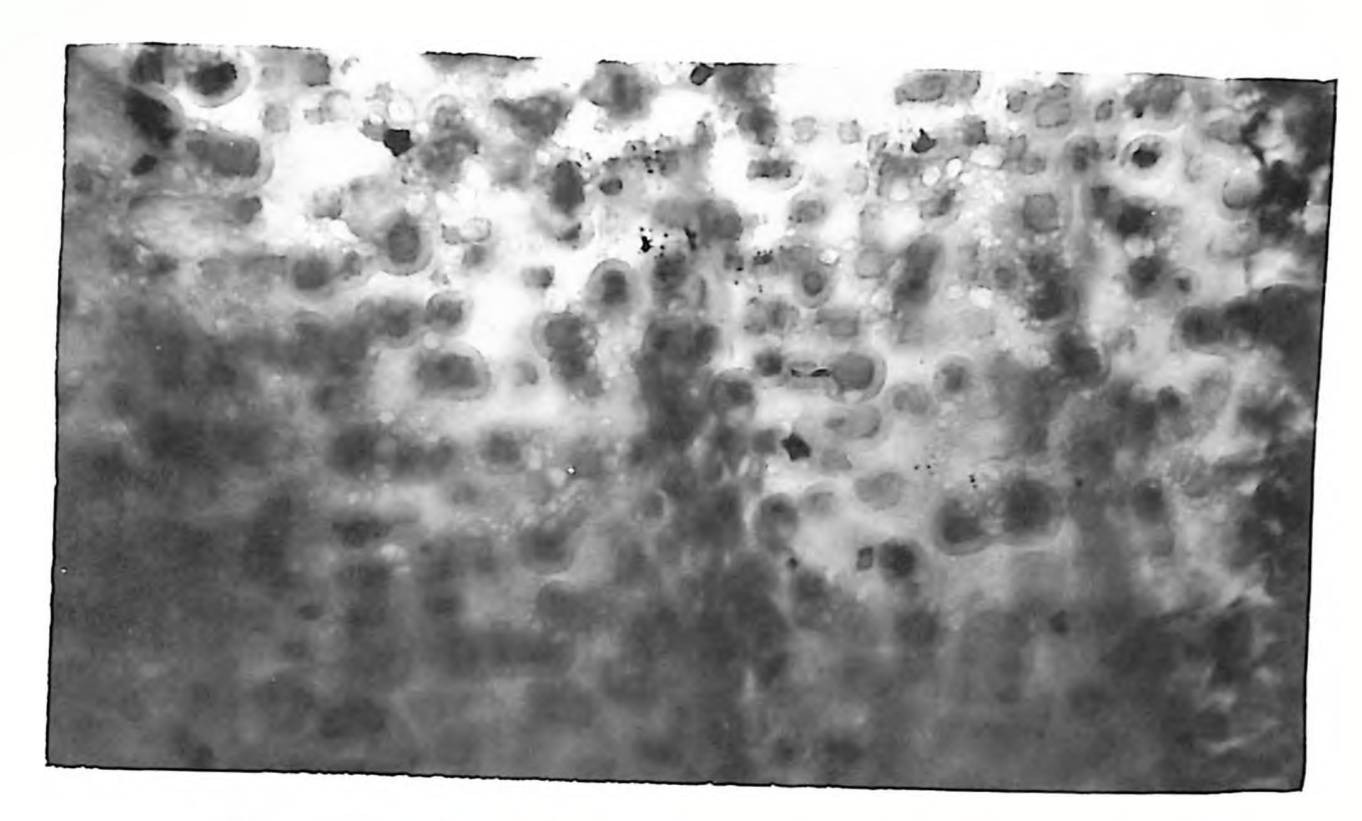


Fig. 21 Microstructure after fatigue, diffraction effect. M210,000

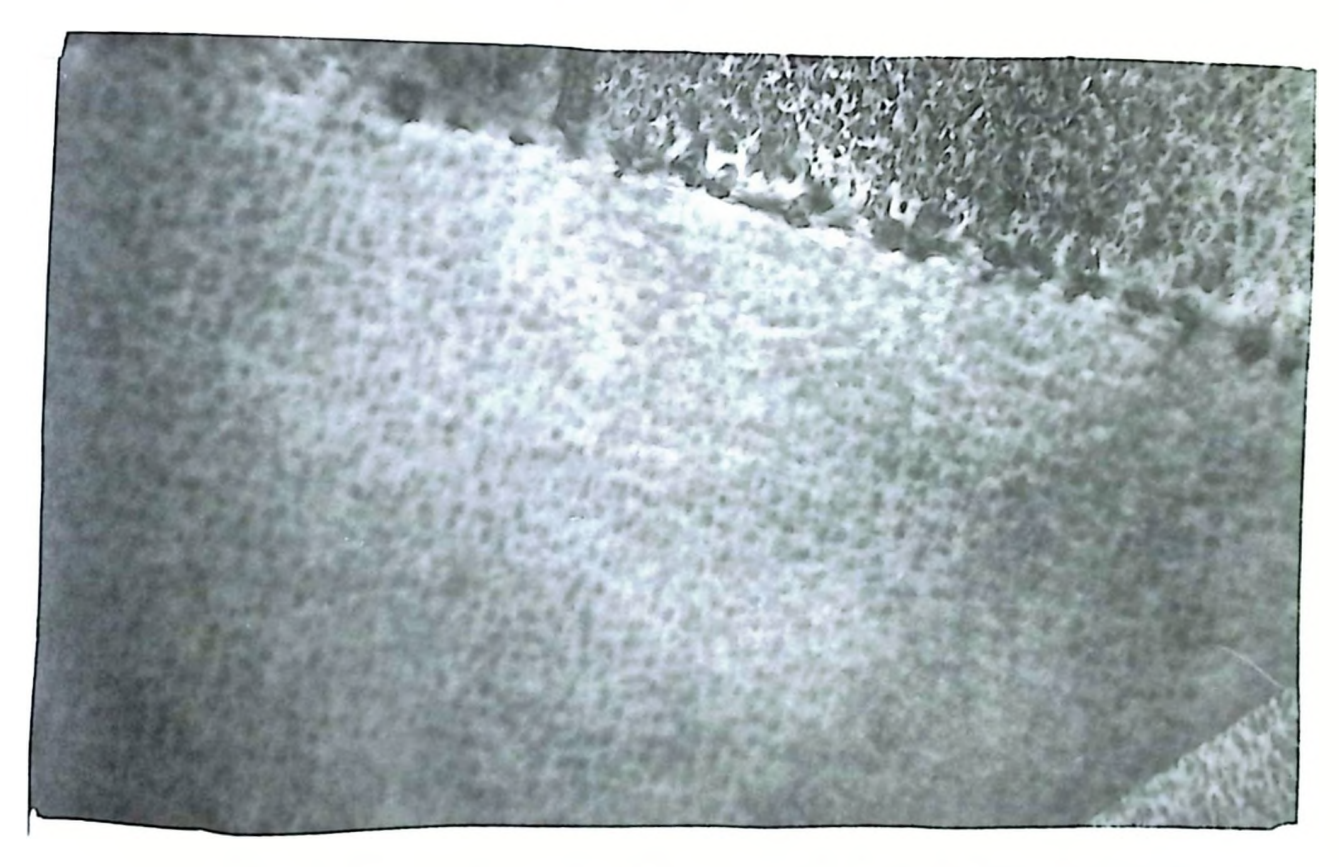


Fig. 24 Precipitate present after 60 minutes at 640°C. x68,000

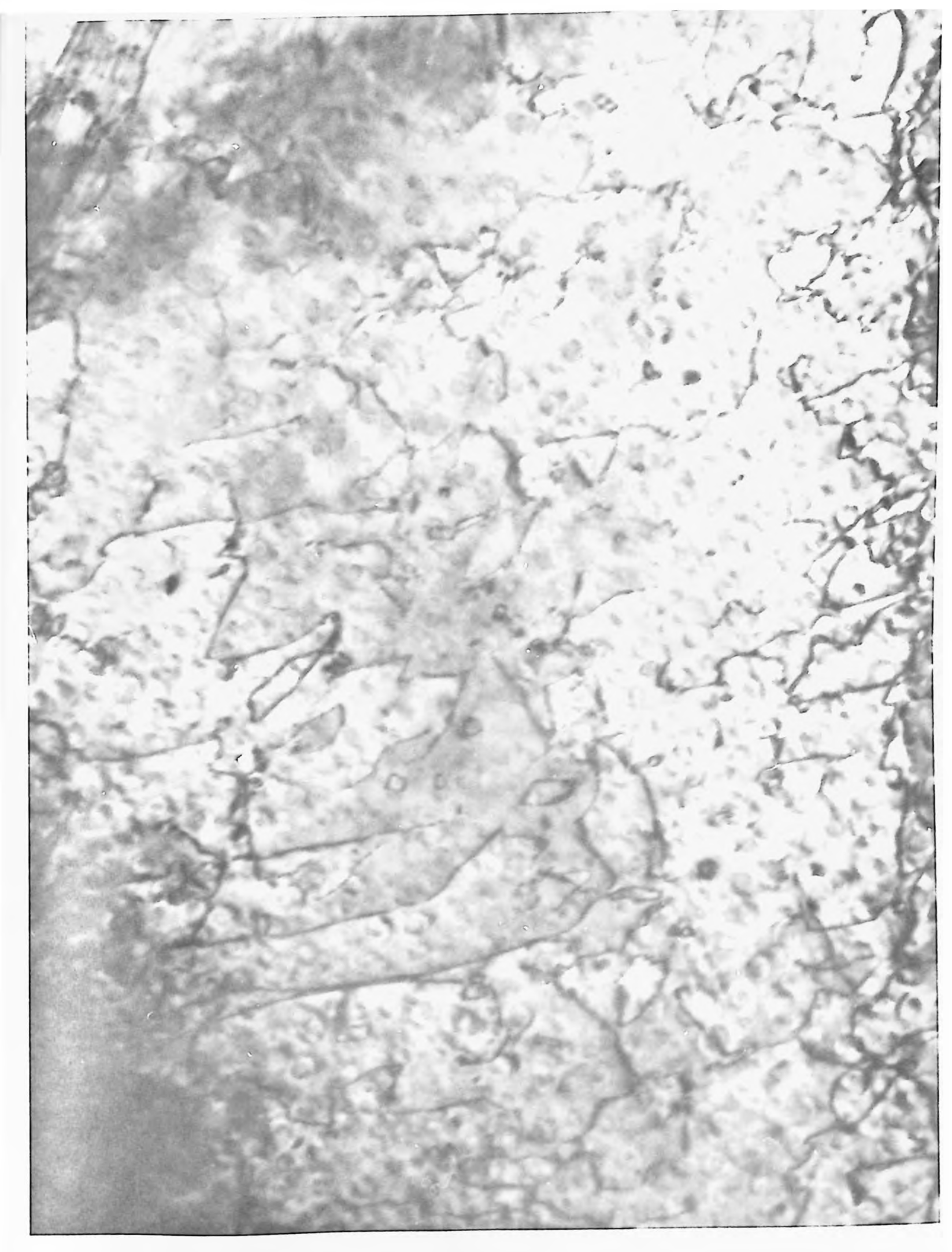


Fig. 23 Precipitate dislocation interaction. X180,000

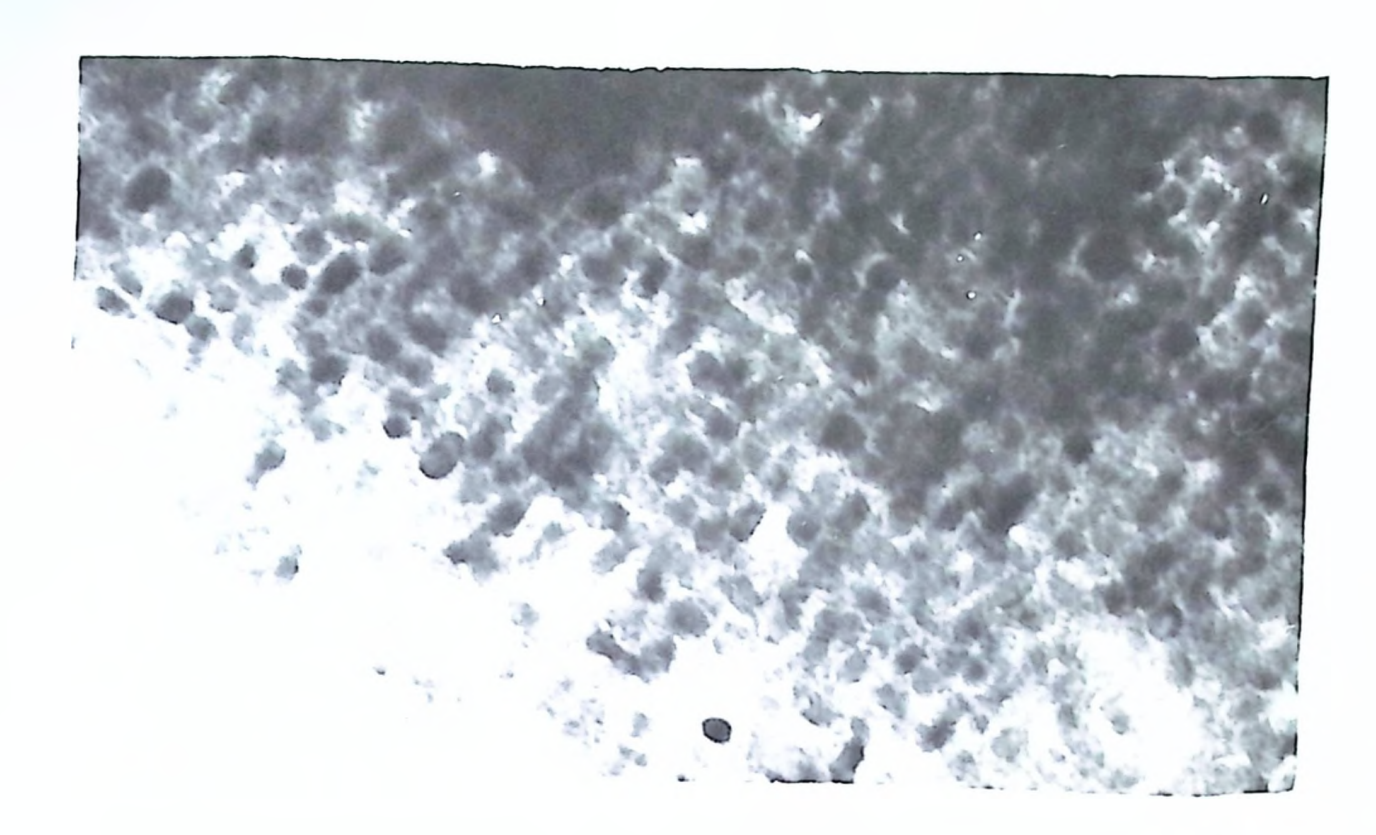


Fig. 25 Modulation present in swaged CuNiFe (heat 7) X220,000

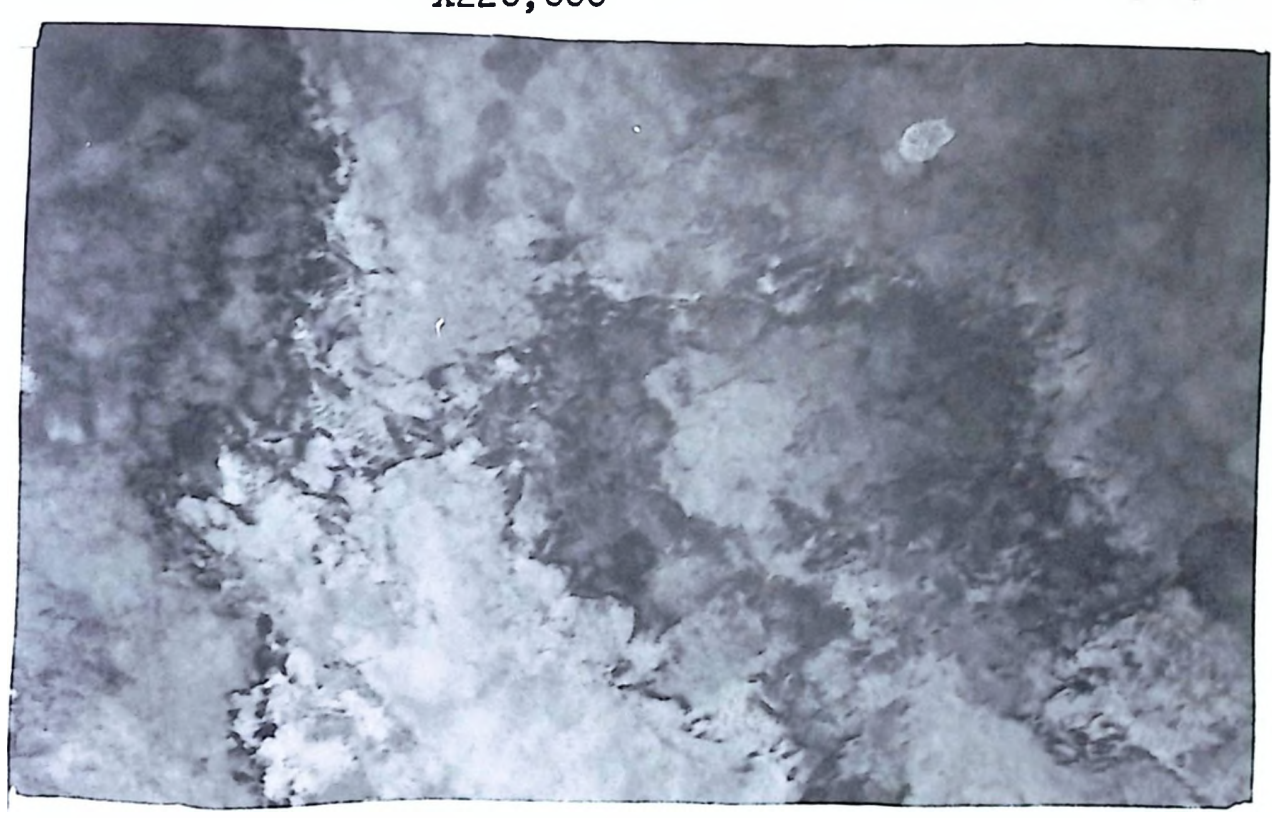


Fig. 26 Swaged CuNiFe, coarse cell structure initially present. X44,000



Fig. 27 Dislocation substructure within coarse cells.

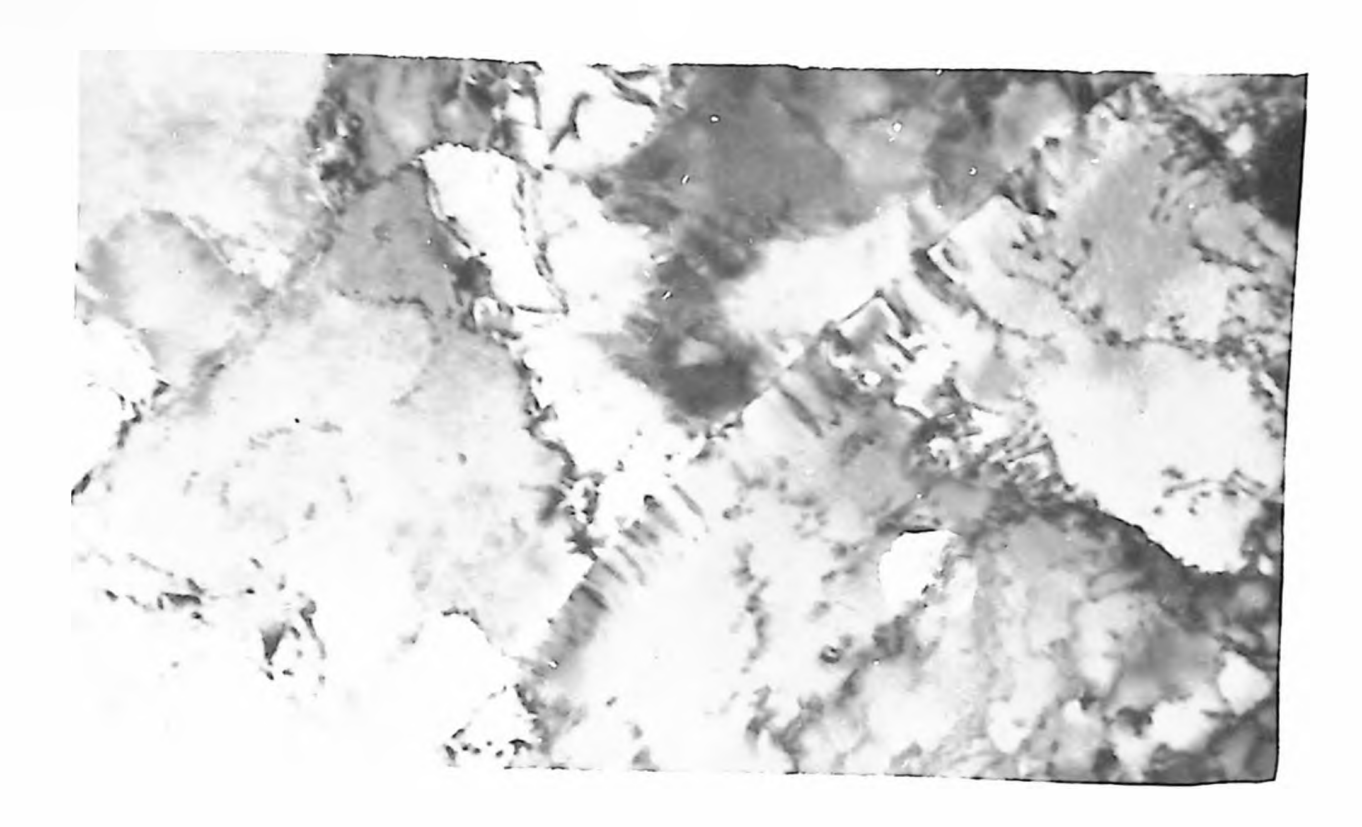


Fig. 28 Heterogeneous precipitate. X75,000

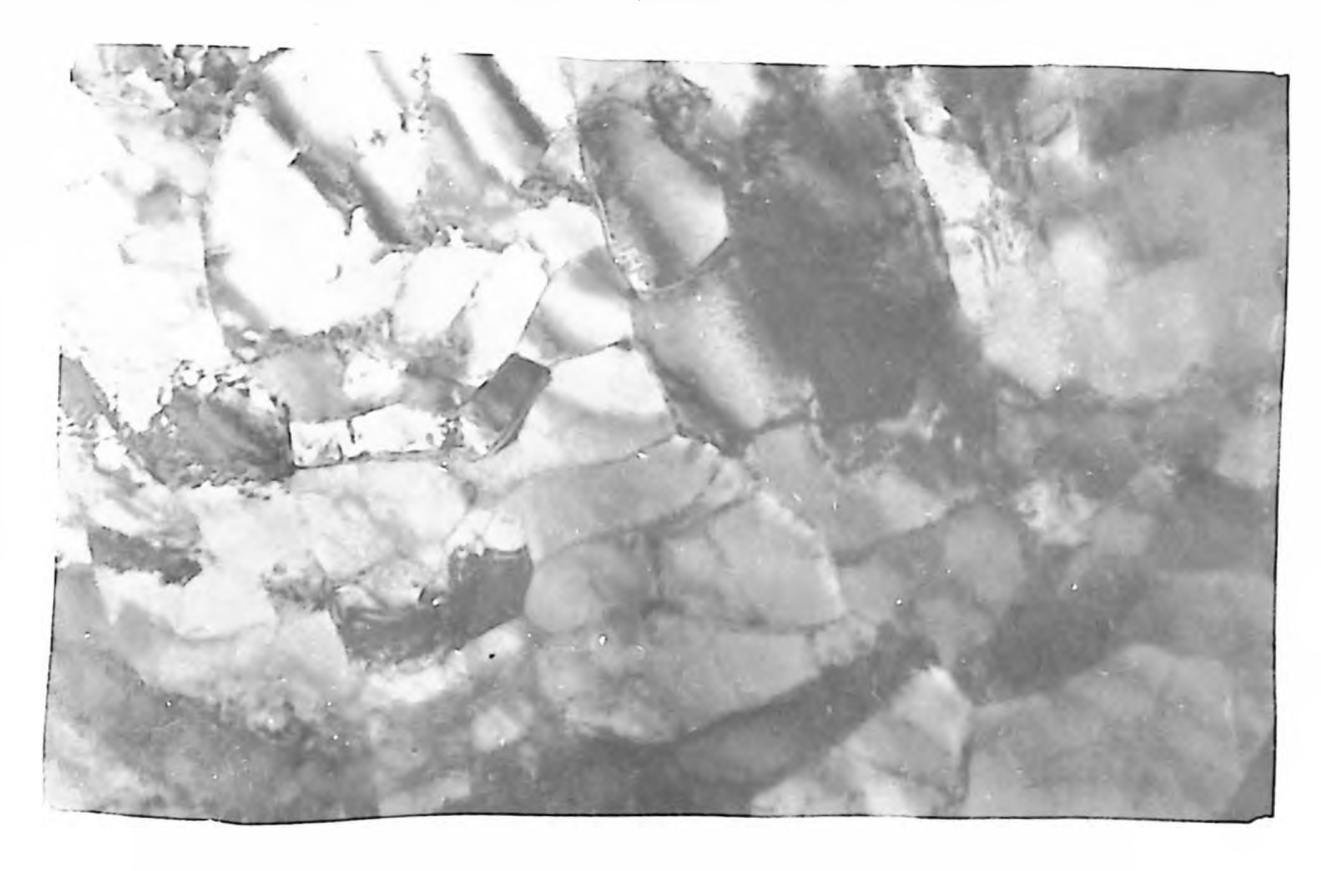


Fig. 29 Refinement of cell structure. X70,000

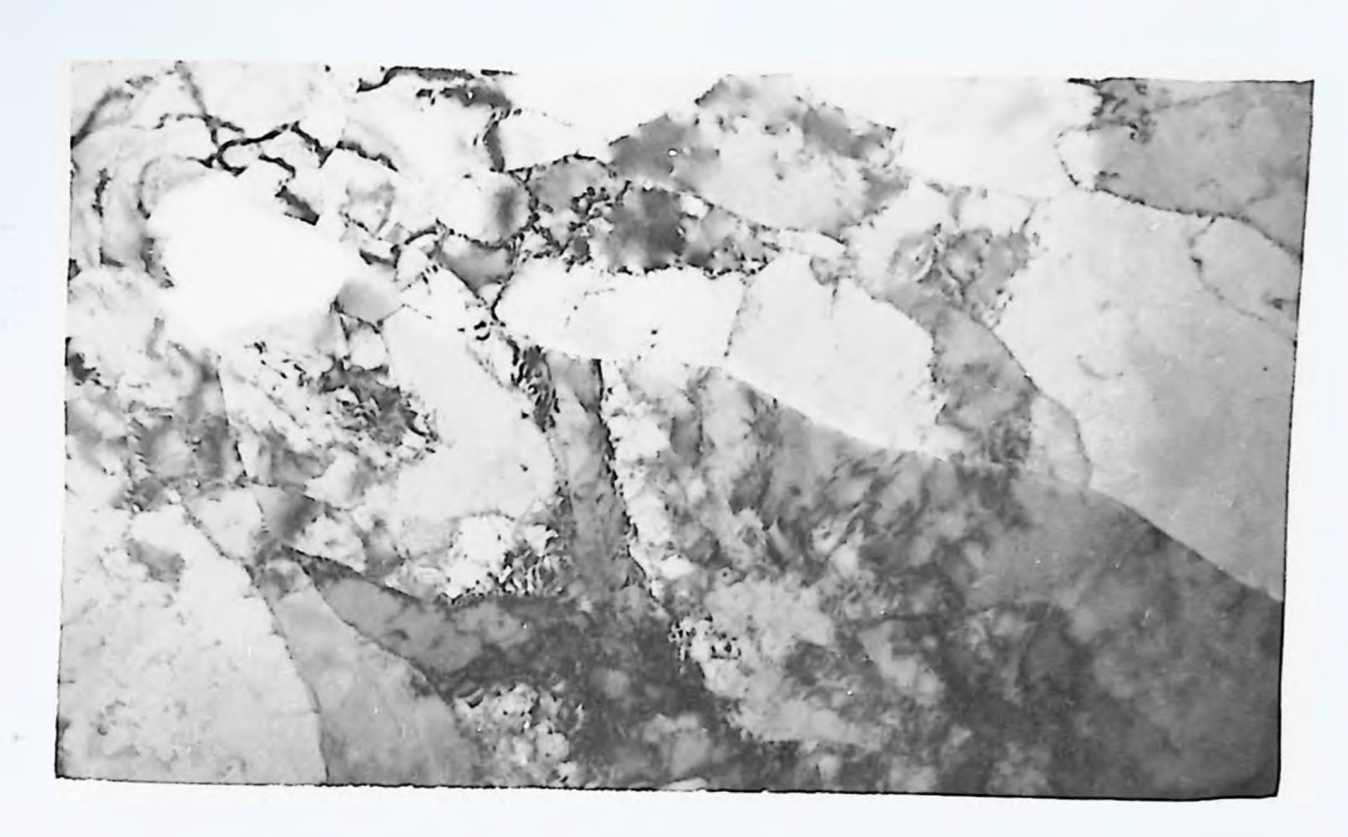


Fig. 30 Refinement of cell structure. X35,000



Fig. 31 Woolly structure. X40,000

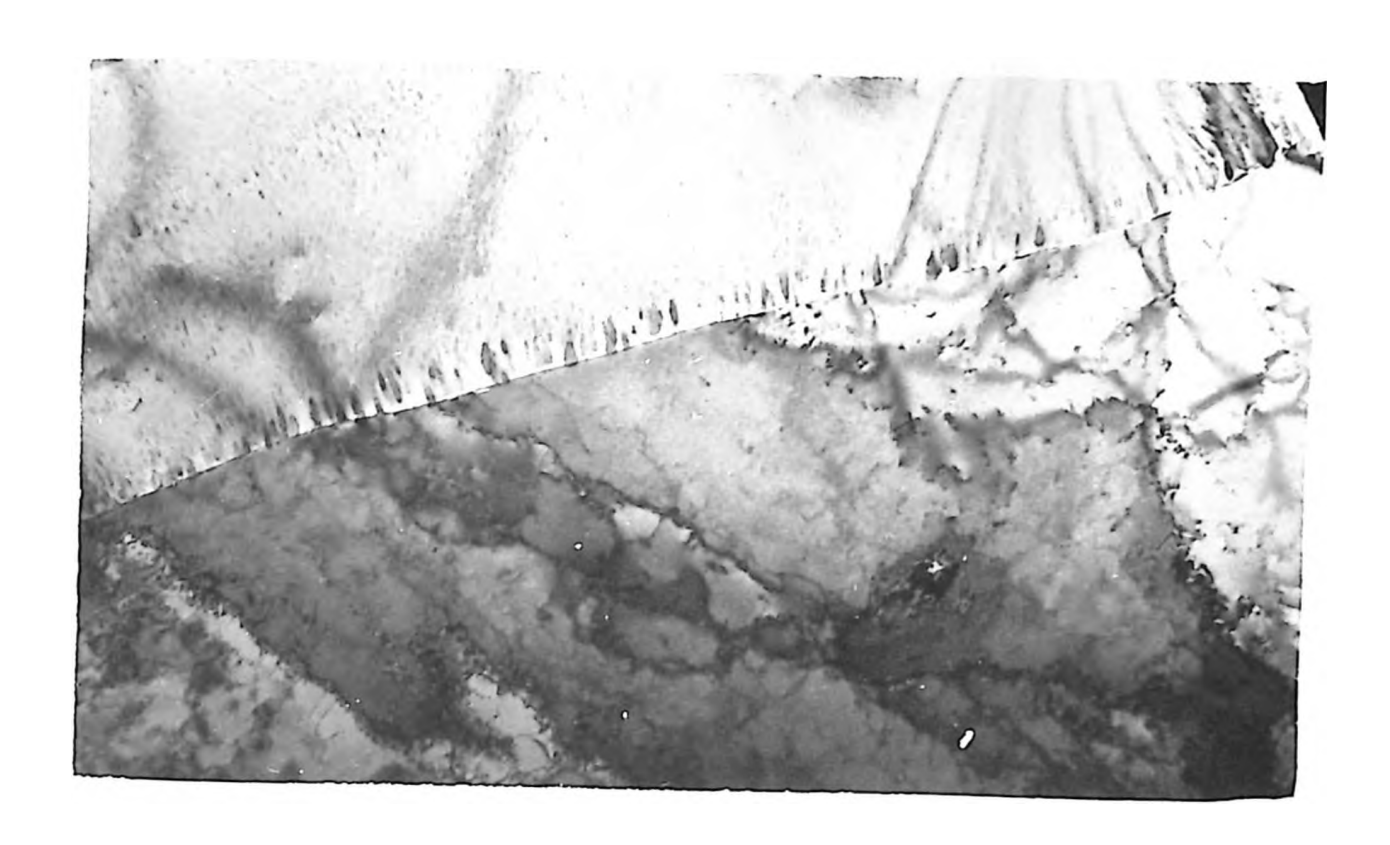


Fig. 32 Heterogeneous precipitate. X38,000



Fig. 33 Heterogeneous precipitate. X40,000



Fig. 34 Twinned area. X32,000

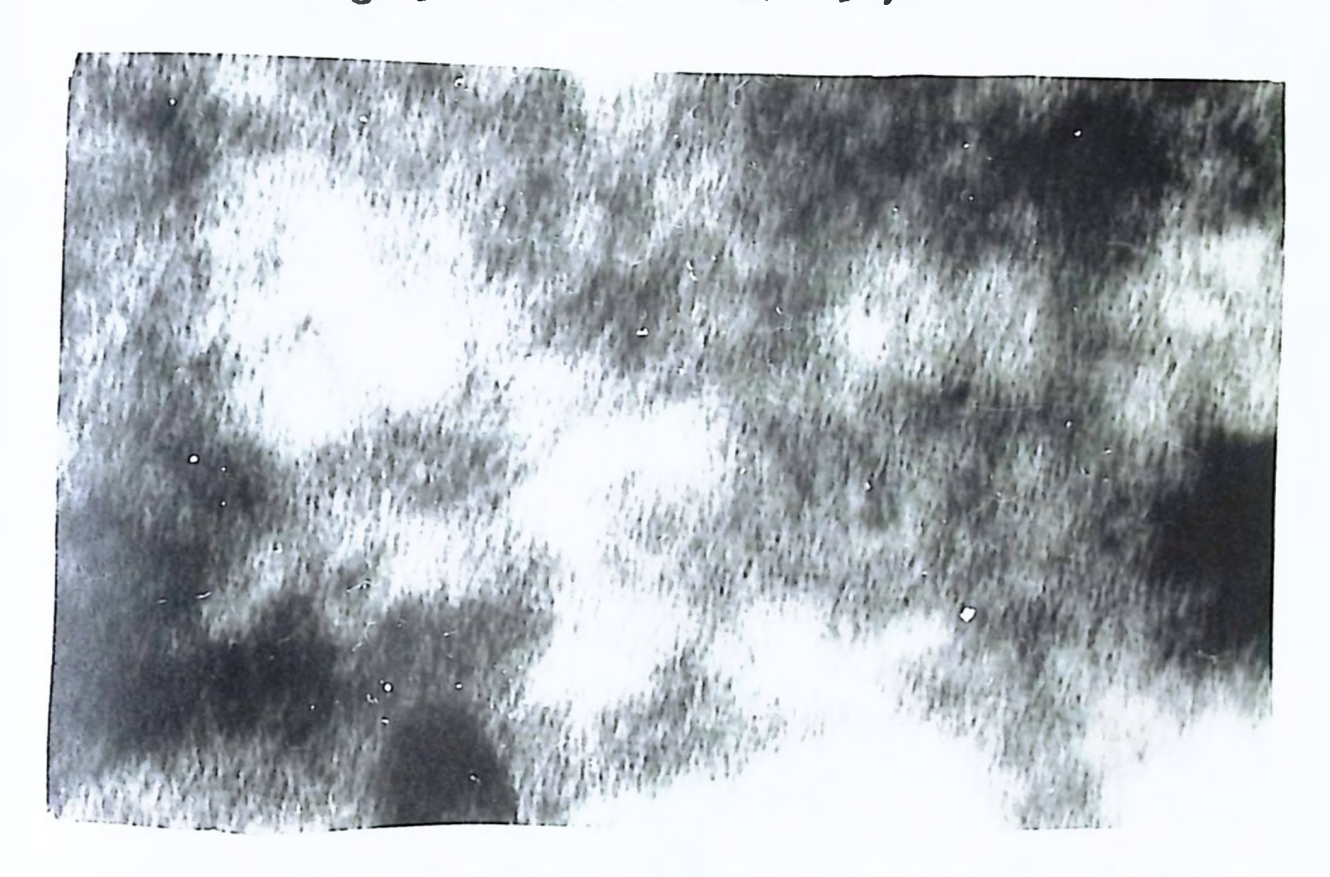


Fig. 35 New modulation after fatigue. X172,000

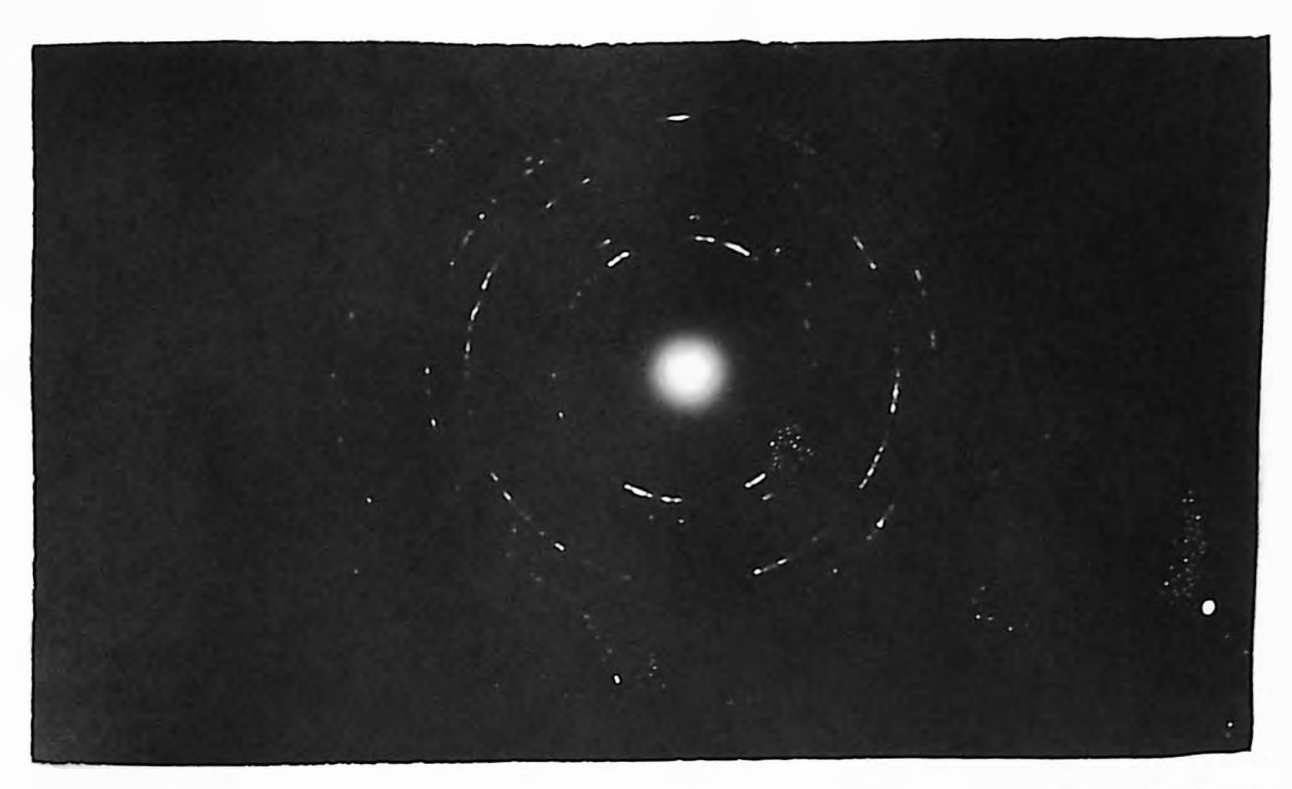


Fig. 36 Diffraction pattern of figure 35, showing typical cellular effect.



Fig. 38 Refinement of cell structure. Mo,000

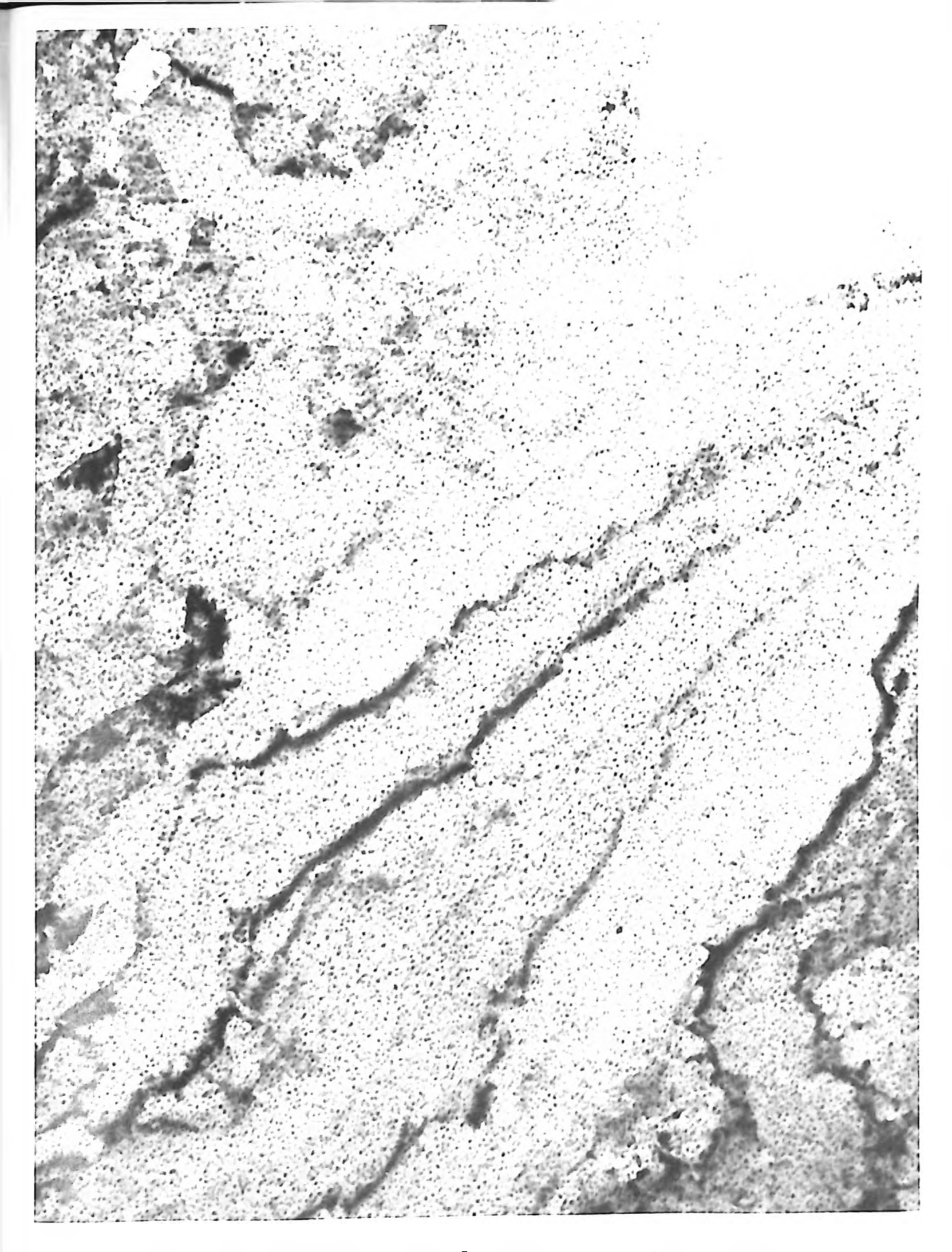


Fig. 37 Structure after 1 month at room temperature. X145,000

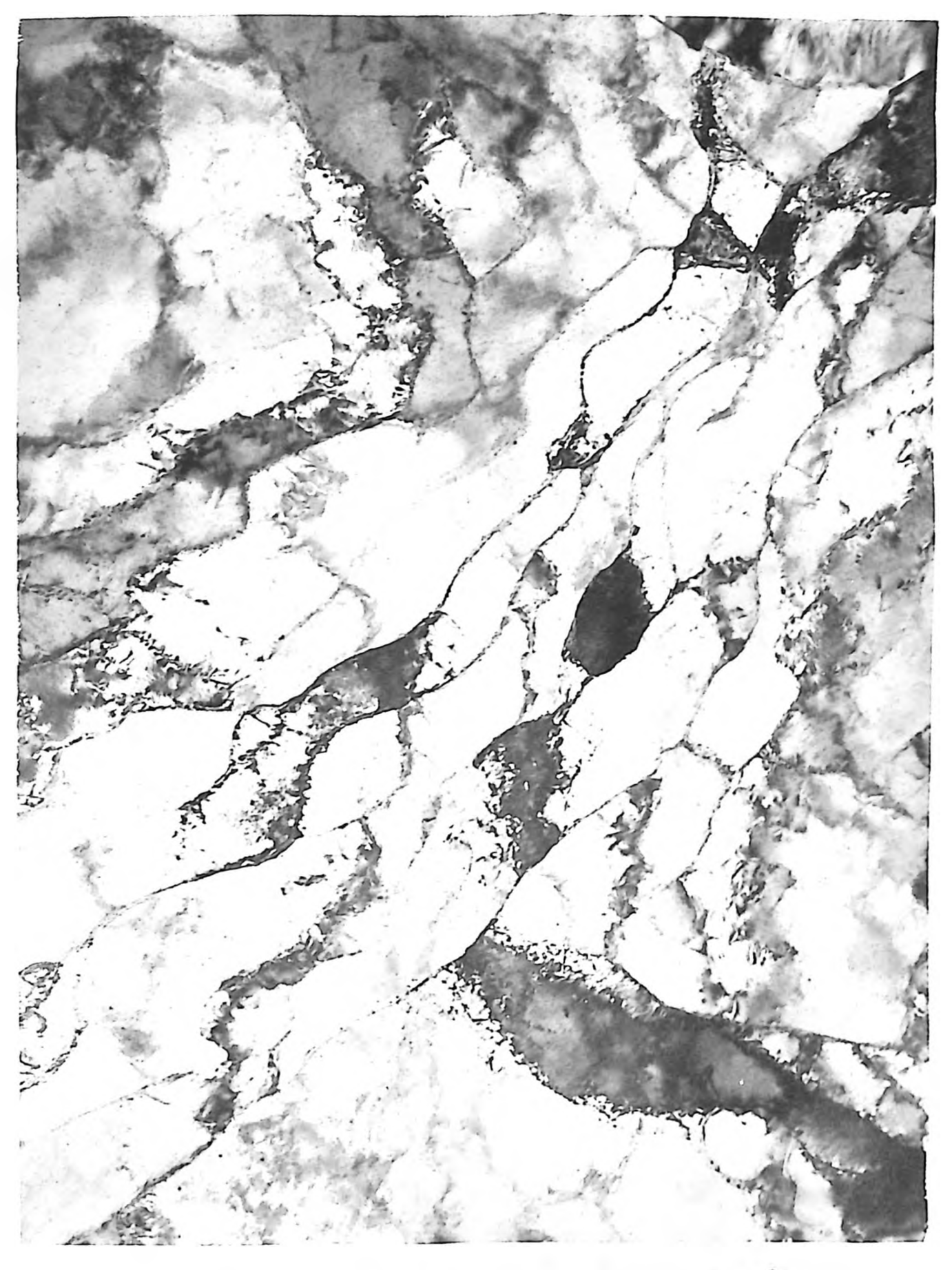


Fig. 39 Refinement of cell structure. %50,000



Fig. 40 Refinement of cell atructure. NG2,000



Fig. 42 Precipitate present after fatigue. X102,000

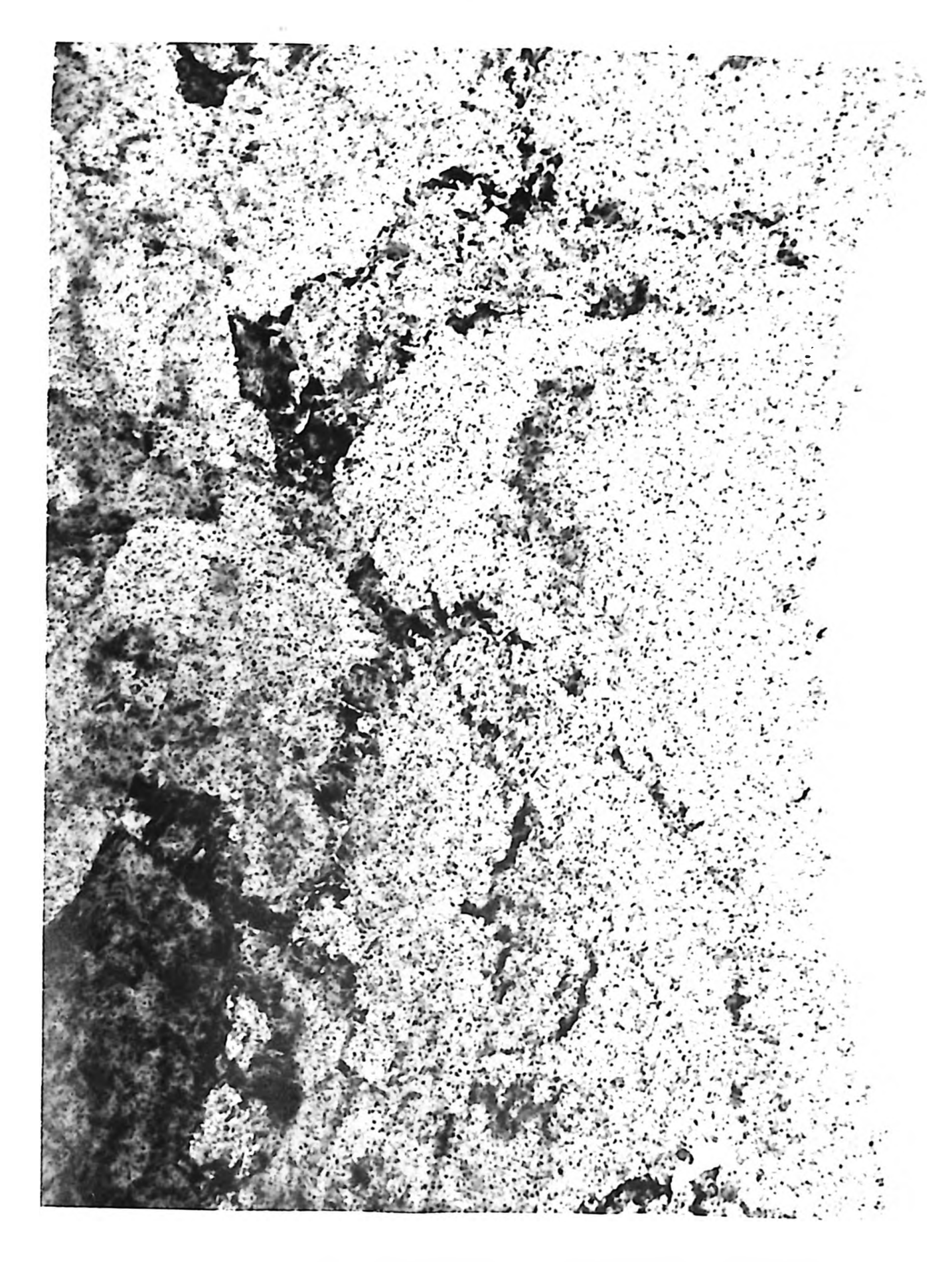


Fig. 43 Precipitate present after fatigue. X105,000

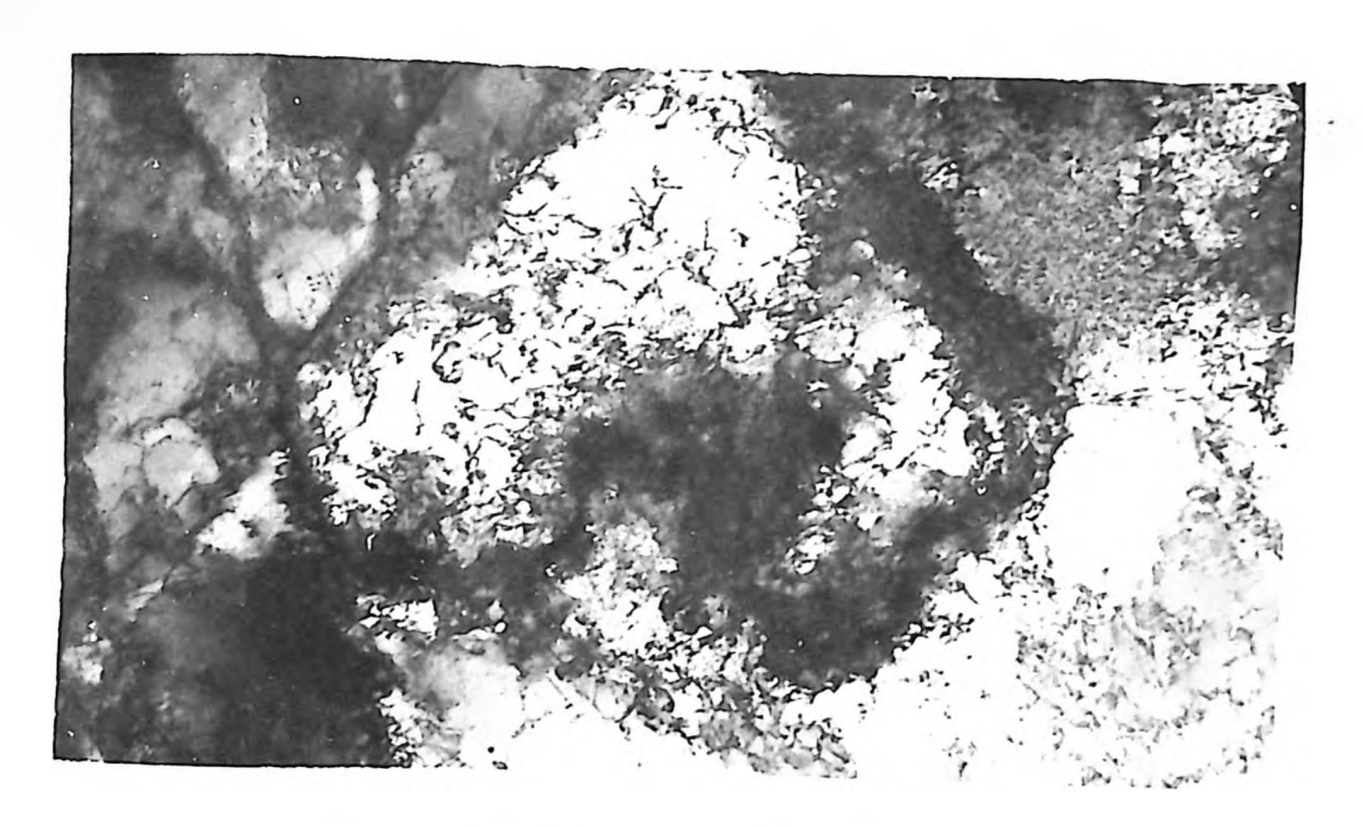


Fig. 41 Woolly structure. X45,000

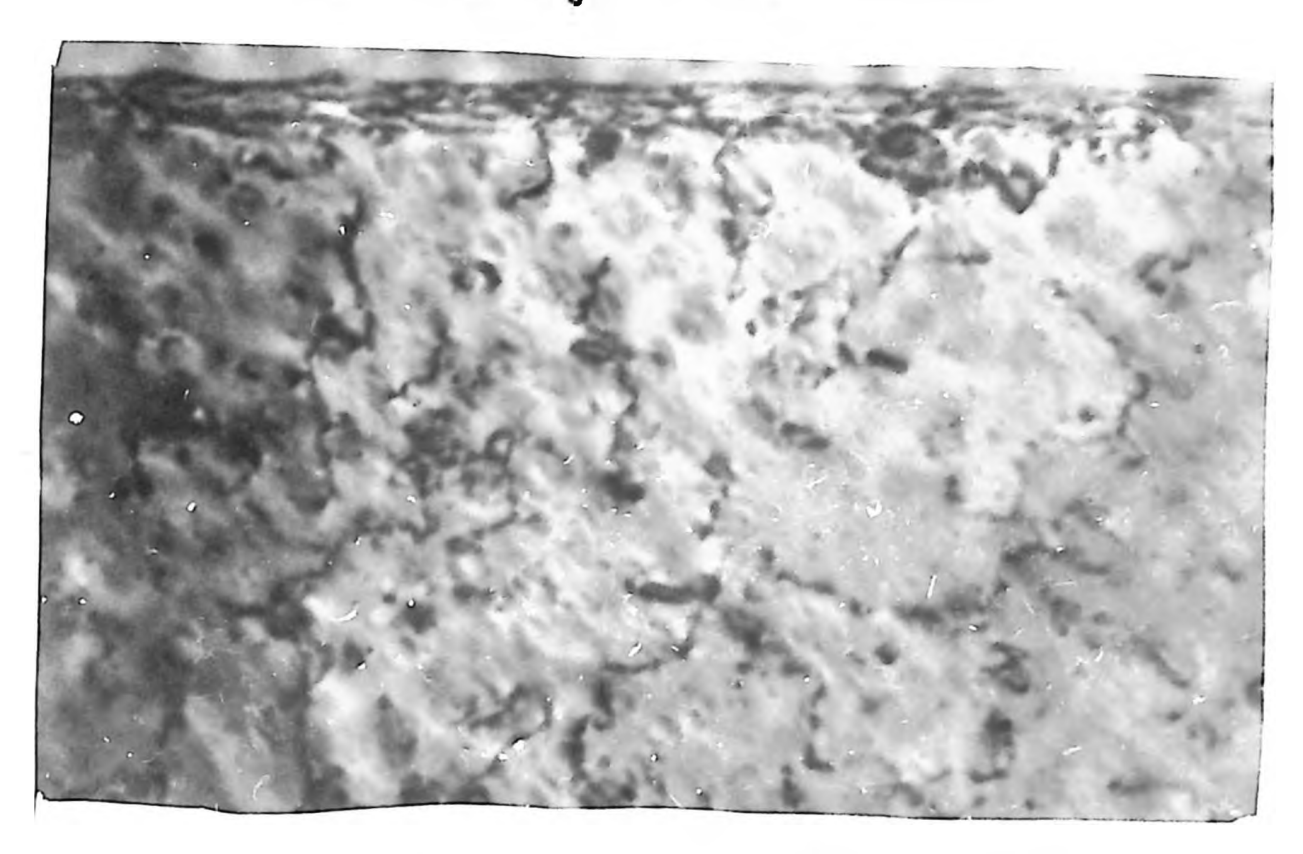


Fig. 44 Dislocation interaction at grain boundary. X120,000